RPW8/HR Repeats Predict NLR-dependent Hybrid Performance

Cristina A. Barragan[1], Rui Wu[1], Sang-Tae Kim[1,3], Wanyan Xi[1], Anette Habring[1], Jörg Hagmann[1,4], Anna-Lena Van de Weyer[1], Maricris Zaidem[1,5], William Wing Ho Ho[1,6], George Wang[1], Ilja Bezrukov[1], Detlef Weigel[1*], Eunyoung Chae[1,2*]

*Corresponding authors: weigel@tue.mpg.de (D.W.), dbsce@nus.edu.sg (E.C.)

[1]Department of Molecular Biology, Max Planck Institute for Developmental Biology, 72076 Tübingen, Germany
[2]Department of Biological Sciences, National University of Singapore, 117558, Singapore

Current addresses:
[3]Center for Genome Engineering, Institute for Basic Science, Daejeon, 34126, South Korea
[4]Computomics GmbH, 72076 Tübingen, Germany
[5]Center for Genomics and Systems Biology, New York University, New York, NY 10003, USA
[6]Melbourne Integrative Genomics, The University of Melbourne, Parkville VIC 3052, Australia

Keywords
RPW8, NLR, natural variation, autoimmunity, hybrid performance, MLKL, HET-S

Summary

Hybrid offspring can look very different from their parents, including having greatly increased or decreased fitness. In many plant species, conflicts between divergent elements of the immune system can cause hybrids to express autoimmunity, a generally deleterious syndrome known as hybrid necrosis. We are investigating multiple hybrid necrosis cases in *Arabidopsis thaliana* that are caused by allele-specific interactions between different variants at two unlinked resistance (R) gene clusters. One is the *RESISTANCE TO PERONOSPORA PARASITICA 7* (*RPP7*) cluster, which encodes an intracellular nucleotide binding site-leucine rich repeat (NLR) immune receptors that confer strain-specific resistance to oomycetes. The other is the *RESISTANCE TO POWDERY MILDEW 8* (*RPW8*)/*HOMOLOG OF RPW8* (*HR*) locus, which encodes atypical resistance proteins that can confer broad-spectrum resistance to filamentous pathogens. There is extensive structural variation in the *RPW8*/*HR* cluster, both at the level of gene copy number and at the level of C-terminal protein repeats of unknown function. We demonstrate that the number of RPW8/HR repeats correlate, albeit in a complex manner, with the severity of hybrid necrosis when these alleles are combined with specific *RPP7* variants. This observation suggests that gross structural differences, rather than individual amino acid polymorphisms, guide the genetic interaction between *RPW8*/*HR* and *RPP7* alleles. We discuss these findings in light of the similarity of RPW8/HR proteins with pore-forming toxins, MLKL and HET-S, from mammals and fungi.

Introduction

The combination of divergent parental genomes in hybrids can produce new phenotypes not seen in either parent. At one end of the spectrum is hybrid vigor, with progeny being superior to the parents, while at the other end there is hybrid weakness, with progeny being inferior to the parents, and in the most extreme cases sterile or unable to survive. Both types of interactions are important in breeding — the first is sought after, while the second must be avoided, even when only very mild.

Disease resistance is one of the most desirable traits in selective crop breeding [1,2], but the outcome of stacking different resistances is unfortunately not always predictable. On the one hand, different genetic backgrounds can lead to suppression or attenuation of disease resistance, and some of this is due to genetic interactions between different disease resistance loci or alleles [3–10]. Conversely, the combination of divergent germplasm, which is an important source of novel variation in breeding, also incurs the risk of genetic incompatibilities. In plants, a particularly conspicuous set of incompatibilities is associated with autoimmunity, often with substantial negative effects on hybrid fitness [11–13]. Studies of hybrid autoimmunity in several species, often expressed as hybrid necrosis, have revealed that the underlying genetics tends to be simple, with often only one or two causal loci. Where known, at least one of the causal loci encodes an immune protein, often an intracellular nucleotide binding site-leucine-rich repeat (NLR) protein [14–23]. The gene family encoding NLR immune receptors is the most variable gene family in plants, both in terms of inter- and intraspecific variation [24–27]. Many NLR proteins function as major disease resistance (R) proteins, with the extravagant variation at these loci being due to a combination of maintenance of very old alleles by long-term balancing selection and rapid evolution driven by strong diversifying selection [28–30]. The emergence of new variants is favored by many NLR genes being organized in tandem clusters, which can spawn new alleles as well as copy number variation by illegitimate recombination, and by the presence of leucine rich repeats in NLR genes, which can lead to expansion and contraction of coding sequences [31–33]. Cluster expansion has been linked to diversification and adaptation in a range of systems [34–36]. Several complex plant NLR loci provide excellent examples of cluster rearrangement increasing pathogen recognition specificities [29].

Substantial efforts have been devoted to decomposing the complexity of the plant immune system and interactions between its components. In maize, the genetic architecture of the hypersensitive response (HR), a common readout for NLR-mediated immunity, was assessed by crossing a test line harboring the autoimmune *NLR*, *Rp1-D21*, to several hundred nested associated mapping (NAM) lines. Using a genome-wide association (GWA) approach, a major quantitative trait locus (QTL) associated with the variation in HR in the F_1 hybrids was found, although the exact causal gene remains unconfirmed [37]. Another aspect of the complexity of the NLR network is reflected by some NLRs relying on signaling by specific executor NLRs, while in other cases, several NLRs make use of overlapping sets of helper NLRs [24–26,38–41]. Finally, NLR gene expression can be modulated by several families of miRNAs that can target – with different efficiency – many NLRs, but that at the same time are also evolutionarily very fluid [42].

While many plant disease R genes are members of the NLR family, some feature different molecular architectures. One of these is *RESISTANCE TO POWDERY MILDEW 8* (*RPW8*) in *Arabidopsis thaliana*, which has an allele that confers resistance to multiple powdery mildew isolates [43]. The namesake *RPW8* gene is located in a gene cluster of variable size and composition that includes multiple *RPW8*-like genes as well as *HOMOLOG OF RPW8* (*HR*) genes [43–45]. The reference accession Col-0, which is susceptible to powdery mildew, has four *HR* genes, but no *RPW8* gene, whereas the resistant accession Ms-0 carries *RPW8.1* and *RPW8.2* along with three *HR* genes [43].

NLRs are distinguished by N-terminal Toll/interleukin-1 receptor (TIR) or coiled-coil (CC) domains, which, when overexpressed alone, can often activate immune signaling [46,47]. A subset of CC-NLRs (CNLs) has a diagnostic type of coiled-coil domain, termed CC_R to indicate that this domain is being shared with RPW8/HR proteins. The latter have an N-terminal extension that might be a transmembrane domain as well as C-terminal repeats of unknown activity [48,49]. It has been noted that the CC_R domain is similar to a portion of the animal mixed-lineage kinase domain-like (MLKL) protein that forms a multi-helix bundle [50] as well as the HeLo and HELL domains of fungi, which also form multi-helix bundles [51–53].

We have previously reported hybrid necrosis due to incompatible alleles at the *RPW8/HR* locus and at the complex *RECOGNITION OF PERONOSPORA PARASITICA 7* (*RPP7*) locus, which encodes a canonical CNL and which has alleles that provide race-specific resistance to the oomycete *Hyaloperonospora arabidopsidis* [54,55]. Here, we investigate in detail three independent cases of incompatible *RPW8/HR* and *RPP7* alleles, and show that two are caused by members of the fast-evolving *RPW8.1/HR4* clade. We describe how variation in the number of C-terminal repeats predicts the degree of incompatibility between two common *RPW8.1/HR4* alleles and corresponding *RPP7* alleles.

Results

Distinct pairs of *RPP7* and *RPW8/HR* alleles causing hybrid necrosis

In a systematic intercrossing and genetic mapping program among 80 *A. thaliana* accessions, the interaction between the *DM6* and *DM7* loci stood out because these two loci were found to be responsible for two phenotypically distinct hybrid necrosis cases between accessions Mrk-0 and KZ10 and accessions Lerik1-3 and Fei-0 (**Figure 1a**) [20]. A combination of mapping, knockdown and transformation with genomic constructs had pointed to *DM6* being encoded by a member of the *RPP7* cluster, and to *DM7* by a member of the *RPW8/HR* cluster. A third case of apparent *DM6–DM7* incompatibility involves accessions ICE79 and Don-0, which shows its own distinctive phenotype (**Figures 1a and 2a**). In addition to the phenotypic differences among the three *DM6–DM7* dependent hybrid necrosis cases (**Figure 1a**), test crosses confirmed the allele specificity of the *DM6–DM7* interactions (**Figure 1b**).

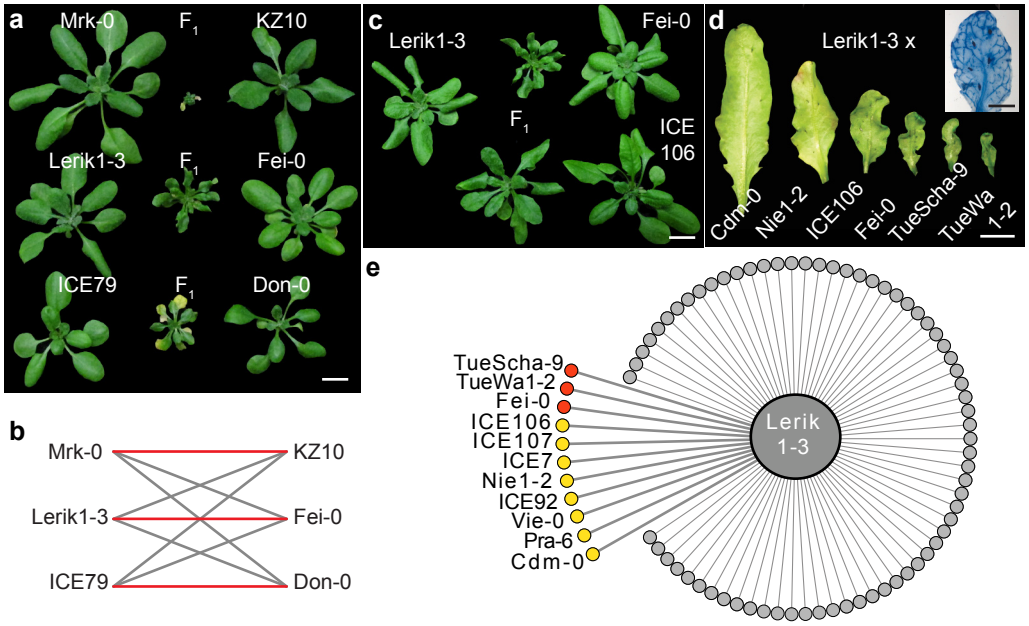

Figure 1. *DM6–DM7* hybrid necrosis cases
(**a**) Variation in morphology in three independent *DM6–DM7* hybrid necrosis cases. (**b**) Red indicates necrosis in F_1 hybrids, black indicates normal progeny. (**c, d**) Variation in morphology in two *DM6–DM7* cases sharing the same *DM6* allele as Lerik1-3. (**c**) Entire rosettes of four week-old plants. (**d**) Abaxial sides of eighth leaves of six-week old plants. Inset shows Trypan Blue stained leaf of Lerik1-3 x Fei-0 F_1. (**e**) Summary phenotypes in crosses of Lerik1-3 to 80 other accessions. Red is strong necrosis in F_1, and yellow is mild necrosis in F_1 or necrosis only observable in F_2. Scale bars indicate 1 cm.

We had previously used artificial microRNAs (amiRNAs) to establish that *DM6*$^{Lerik1-3}$ was encoded by a particular loci in the complex *RPP7* cluster of NLR genes, which is highly variable between natural accessions [56]. To corroborate the evidence from mapping experiments that *DM6*$^{Mrk-0}$ and *DM6*^{ICE79} were also caused by *RPP7* homologs, we designed ten amiRNAs based on the sequences of eight *RPP7* homologs found in the genome of the reference accession Col-0. AmiRNAs targeting a subclade of *RPP7* homologs, *At1g58602*, *At1g58807*, *At1g58848*, *At1g59124* and *At1g59218*, which make up the second half of the *RPP7* cluster, suppressed hybrid necrosis in all three crosses, Mrk-0 x KZ10, Lerik1-3 x Fei-0 and ICE79 x Don-0. AmiRNAs targeting the genes of the first half of the cluster, *At1g58390*, *At1g58400* and *At1g48410*, did not (**Figure S1 and Table S1**). These rescue experiments, together with the above-mentioned test crosses, indicate that specific *RPP7* homologs in Mrk-0, Lerik1-3 and ICE79 correspond to different *DM6* alleles that cause hybrid necrosis in combination with specific *DM7* alleles from other accessions.

A common set of *RPW8/HR* alleles affecting hybrid performances in F_1 and F_2 progeny

In a set of diallelic F_1 crosses among 80 accessions [20], we noted that Lerik1-3, which carries a *DM6* (*RPP7*) hybrid necrosis risk allele, was incompatible with several other accessions, suggesting that these carry *DM7* (*RPW8/HR*) risk alleles that are similar to the one in Fei-0. Crosses with TueScha-9 and TueWa1-2 produced hybrids that looked very similar to Lerik1-3 x Fei-0 progeny, what we had previously defined as class 2 hybrid

necrosis, with localized spots of cell death spread across the leaf lamina along with leaf crinkling and dwarfism (**Figures 1d and S2**). Similar spots of cell death and leaf crinkling were also observed in crosses of Lerik1-3 to ICE106 and ICE107, although these were not as dwarfed and had therefore been classified as class I hybrid necrosis (**Figures 1c,d and S2**).

Table 1. F_2 segregation ratios at 16°C

Cross	n[a]	Phenotype				Model[d]	χ^2
		Normal[b]	F_1-like[b]	Enhanced[c]			
Fei-0/Lerik1-3	384	178	107	99		I	0.85
TueWa1-2/Lerik1-3	138	66	42	30		I	0.36
TueScha-9/Lerik1-3	193	92	44	57		I	0.42
Lerik1-3/ICE106	265	121	67	62	15	II	0.89
Lerik1-3/ICE107	291	204		70	17	III	0.88
Cdm-0/Lerik1-3	260	173		71	16	III	0.68
Nie-0/Lerik1-3	227	170		57		IV	0.59

a. If the model had a class of dead segregants that could not be counted, *n* was estimated to include the dead individuals for χ^2 calculation.
b. In the bottom three populations, F_1 phenotypes were nearly indistinguishable from normal ones and therefore both classes were combined.
c. More severe than F_1 hybrids with distinct *DM6–DM7* phenotypes. For milder cases, the enhanced phenotypic classes were separated into two groups, with a rosette diameter of 1 cm as threshold. The rightmost numbers indicate the most severe class.
d. Best-fit models using F_2 segregation analyses with incompatibility alleles indicated as "A" and "B".
   I: two-loci-semi-dominant; F_1-like AaBb; stronger AABb and AaBB; AABB dead and not countable.
   II: two-loci-semi-dominant; F_1-like was AaBb; stronger AABb; AaBB and AABB were almost dead but countable.
   III: two-loci-semi-dominant; Normal and F_1-like indistinguishable; stronger AABb and AaBB; AABB almost dead but countable.
   IV: two-loci-semi-dominant; Normal and F_1-like indistinguishable; stronger AABb and AaBB; AABB dead and not countable.

Hybrid necrosis generally is more severe in the F_2 generation when the causal loci are homozygous [15,17,20,22], and this is also true for the Lerik1-3 x Fei-0 cross (**Table 1**). To explore whether Lerik1-3 might cause even milder forms of hybrid necrosis, we therefore surveyed additional F_2 populations from the panel of 80x80 diallelic crosses involving Lerik1-3. Six of these segregated necrotic plants with very similar phenotypes (**Figures 1d, e and S2**). The F_2 segregation ratios suggest that $DM7^{ICE106}$ is weaker than the *DM7* alleles of Fei-0, TueWa1-2 and TueScha-9, but stronger than the ones from Cdm-0 and Nie-0 (**Table 1**). The 11 *DM7* carriers were not from a particular geographic area, but spread over much of Eurasia (**Figure 1e**).

The phenotypic variation among hybrid necrosis cases involving Lerik1-3 could reflect that the incompatible accessions carry different *DM7* (*RPW8/HR*) alleles, that they carry second-site modifiers, or that they interact with other genes than *DM6* in Lerik1-3. To distinguish between these and other possibilities in an unbiased manner, we carried out linkage mapping with F_3 individuals from Lerik1-3 x ICE106 and Lerik1-3 x ICE107 crosses. We used F_3 populations in order to better distinguish different phenotypic classes, since we

did not know how many causal genes were involved and whether they acted dominantly, semi-dominantly or recessively. A total of 330 F_3 plants, derived from 12 Lerik1-3 x ICE106 and 10 Lerik1-3 x ICE107 F_2 plants, were genotyped using Restriction Associated DNA sequencing (RAD-seq), followed by QTL analysis [57]. Both crosses identified the *DM6* and *DM7* genomic regions as interacting epistatically to produce hybrid necrosis (**Figure 2a, b**).

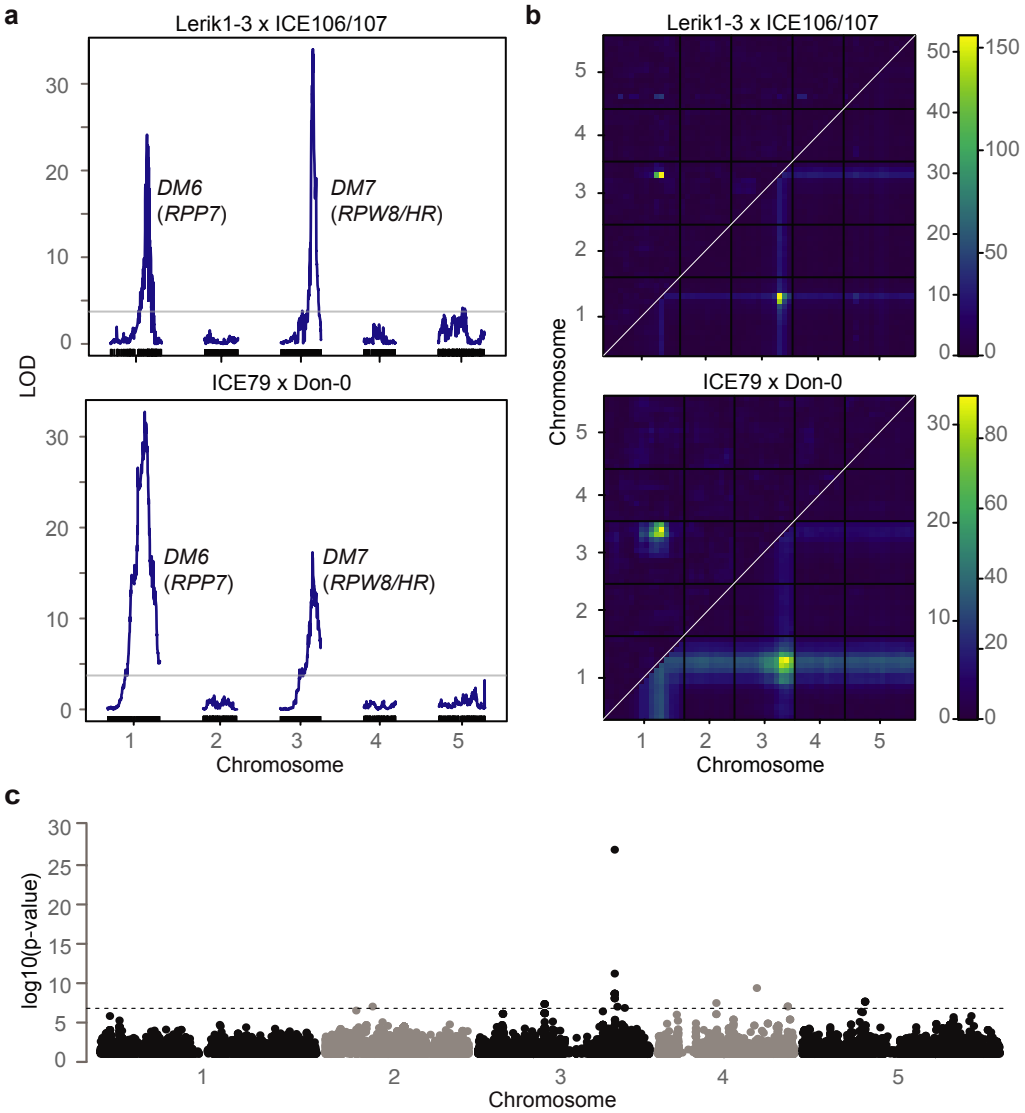

Figure 2. Mapping of two *DM6*–*DM7* hybrid necrosis cases
(**a**) QTL analyses. The QTL on chromosome 1 includes *RPP7* from Lerik1-3 and ICE79 (21.37-22.07 and 21.50-21.98 Mb), and the QTL on chromosome 3 *RPW8/HR* from ICE106/ICE107 and Don-0 (18.59-19.09 Mb, 18.61-19.06 Mb). The horizontal lines indicate 0.05 significance thresholds established after 1000 permutations. (**b**) Heat map for two-dimensional, two-QTL model genome scans. Upper left triangles indicate epistasis scores (LOD*i*) and lower right triangles joint two-locus scores (LOD*f*). Scales for LOD*i* on left and for LOD*f* on right. (**c**) Manhattan plot for a GWAS of necrosis in hybrid progeny of Lerik1-3 crossed to 80 other accessions (see Table S3).

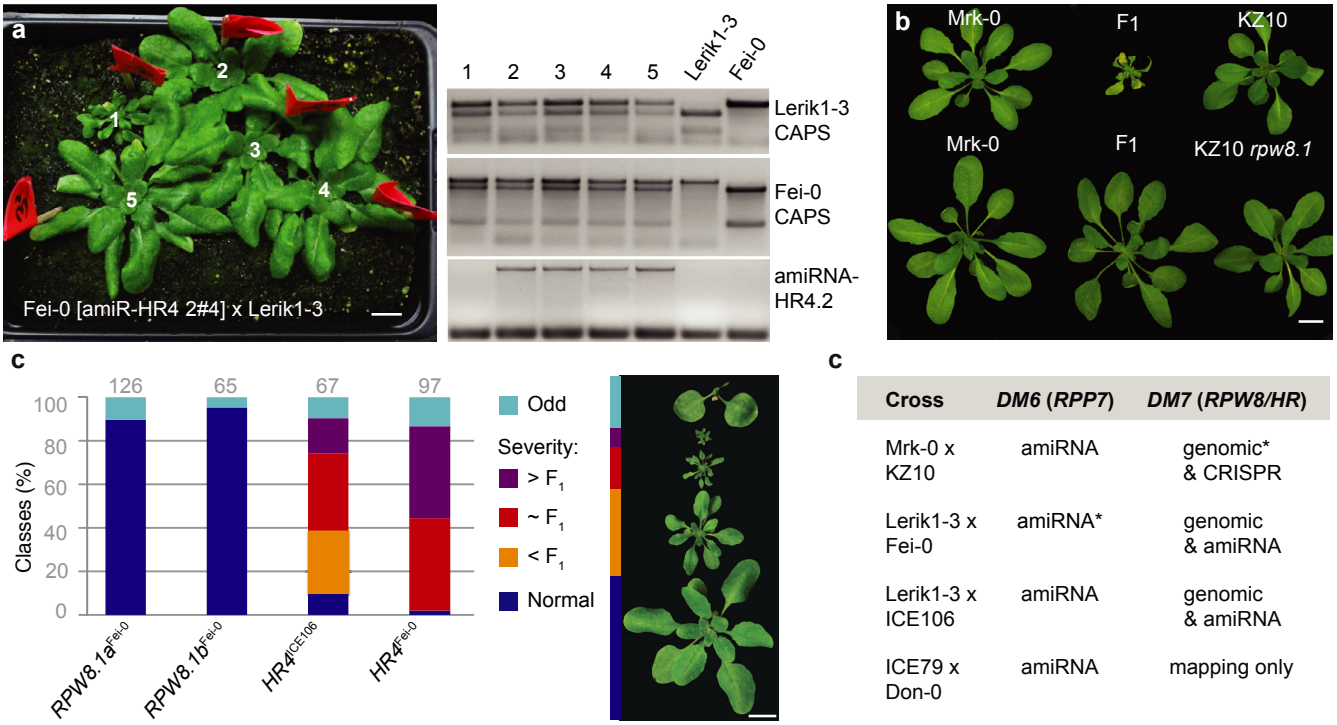

c

Cross	*DM6* (*RPP7*)	*DM7* (*RPW8/HR*)
Mrk-0 x KZ10	amiRNA	genomic* & CRISPR
Lerik1-3 x Fei-0	amiRNA*	genomic & amiRNA
Lerik1-3 x ICE106	amiRNA	genomic & amiRNA
ICE79 x Don-0	amiRNA	mapping only

Figure 3. Confirmation of causal genes in *RPW8/HR* cluster
(**a**) Rescue of hybrid necrosis in Lerik1-3 x Fei-0 F_1 plants with an amiRNA against *HR4*. Fei-0 parents were T_1 transformants. PCR genotyping of numbered plants from left shown on the right. Only plant 1, which does not carry the amiRNA, is necrotic and dwarfed. (**b**) Rescue of hybrid necrosis in Mrk-0 x KZ10 F_1 plants by CRISPR/Cas9-targeted mutagenesis on *RPW8.1*^{KZ10}. (**c**) Recapitulation of hybrid necrosis in Lerik1-3 T_1 plants transformed with indicated genomic fragments from Fei-0 and ICE106. Representative phenotypes on right. Numbers of T_1 plants examined given on top. (**d**) Summary of rescue and recapitulation experiments. Asterisks refer to published experiments [20]. Scale bars indicate 1 cm.

In order to narrow down the *DM7* mapping interval, we took advantage of having 11 accessions that produced hybrid necrosis in combination with Lerik1-3, and 69 accessions (including Lerik1-3 itself) that did not among the 80 accessions from the diallel panel. We used Lerik1-3-dependent hybrid necrosis as a binary trait and performed a GWAS [58]. A clear peak with a maximal $-\log_{10}$(p-value) of 27 was found downstream of the *RPW8/HR* cluster. The most strongly associated single nucleotide polymorphism (SNP) was in the intergenic region following *HR4* (*At3g50480*), the last member of the *RPW8/HR* cluster in the reference accession Col-0 (**Figure 2c and Table S2**).

Based on sequence information from Col-0, Ms-0 and KZ10, we designed amiRNAs targeting different members of the *RPW8/HR* cluster and introduced these into necrotic hybrids. An amiRNA matching *HR4* sequences from Col-0 fully rescued both the strong necrosis in Lerik1-3 x Fei-0 and the weaker necrosis in Lerik1-3 x ICE106 (**Figures 3a and Table S3**). We confirmed the causality of another member of the *RPW8/HR* cluster in the KZ10 x Mrk-0 case with a CRISPR/Cas9-induced mutation of *RPW8.1*^{KZ10} (**Figures 3b and S3**).

Naturally, we wanted to learn what the relationship, if any, is between *RPP7*-dependent hybrid necrosis and the previously described function of certain *RPP7* alleles in conferring resistance to *H. arabidopsidis*. The

RPP7^{Col-0} allele makes Col-0 resistant to the *H. arabidopsidis* isolate Hiks1 [59]. We found Lerik1-3, which carries the *RPP7*$^{Lerik1-3}$ risk allele, but not Fei-0 and ICE106, which do not carry *RPP7* risk alleles, to be resistant to Hiks1 as well (**Figure S6 and Table S9**). Both Lerik1-3 x Fei-0 and Lerik1-3 x ICE106 F_1 hybrids were resistant to Hiks1, although apparently somewhat less so than the Lerik1-3 parents (**Figure S6**). We further tested whether *RPP7*-like genes from Lerik1-3 are likely to be involved in Hiks1 resistance by inoculating Hiks1 on transgenic lines carrying seven different amiRNAs against *RPP7* homologs (**Table S1**), but none of the amiRNAs reduced Hiks1 resistance. These negative results are difficult to interpret; the amiRNAs might not efficiently knock down all *RPP7* homologs in Lerik1-3 (for which the exact structure of the *RPP7* cluster is unknown), Hiks1 resistance in Lerik1-3 might not require *RPP7*, or Hiks1 resistance might be complex, as found in other accessions [60]. Finally, given the interaction of *RPP7* with *RPW8/HR* in hybrid necrosis, we also tested whether *HR4* is required for *RPP7*-mediated Hiks1 resistance in Col-0. Two independent *hr4* CRISPR/Cas9 knockout lines in were generated Col-0 (**Figure S3**), but both remained completely resistant to Hiks1 (**Figure S6 and Table S9**), indicating that *HR4* in Col-0 is not required for *RPP7*-mediated resistance to Hiks1.

Structural variation of the *RPW8/HR* cluster

We previously reported the *RPW8/HR* cluster from KZ10, which carries the risk allele interacting with *RPP7*$^{Mrk-0}$, and which includes one gene, *RPW8.3*, that has no clear orthologs in Col-0 or Ms-0 [20]. Assembly of the *RPW8/HR* cluster from TueWa1-2 which, like Fei-0, carries the risk allele that interacts with *RPP7*$^{Lerik1-3}$, revealed that it has at least 12 *RPW8/HR*-like genes (**Figure 4a**), but the extreme degree of recent duplications did not allow for closure of the assembly from PCR products. Recapitulation experiments identified *HR4*$^{Fei-0}$ as the causal gene for hybrid necrosis (**Figures 3c-d and S4**). The *RPW8/HR* cluster in TueWa1-2 is syntenic with the first four genes in the KZ10 cluster but beyond, synteny is disrupted by several tandem duplications (**Figure 4a**). For example, there are at least four copies of *RPW8.3*-like genes with 93 to 99.8% sequence similarity and two identical *RPW8.1a* genes. One gene, *RPW8.1b*, has an early stop codon.

We analyzed the phylogenetic relationship of the *RPW8/HR* genes in TueWa1-2 with the ones from published *RPW8/HR* clusters in *A. thaliana*, in *A. lyrata* and in *Brassica* spp. [20,44,45,61]. In *A. thaliana*, *RPW8/HR* genes seem to have undergone at least three duplication events, the first one generating a new *A. thaliana* specific clade, followed by independent *RPW8.1/HR4* and *RPW8.2/RPW8.3* duplications. Notably, the *RPW8.1/HR4* clade has the longest branch lengths in the tree, compatible with this clade being particularly prone to hybrid incompatibility (**Figure 4b**). The *RPW8/HR* cluster of TueWa1-2 consists of *RPW8/HR* members from both the ancestral and the two *A. thaliana* specific clades, an arrangement that has not been observed before. Using species-wide data [62], we found that accessions carrying Col-0-like *HR4* alleles have simple cluster configurations, while accessions with *HR4* genes resembling hybrid necrosis alleles have more complex configurations (**Figure 4a**). The tagging SNPs found in GWAS (**Figure 4a, and Table S2**) were

mostly found in the complex, not in the simpler clusters, suggesting that it is linked to structural variation in the distal region of the *RPW8/HR* cluster (**Figure 4b**).

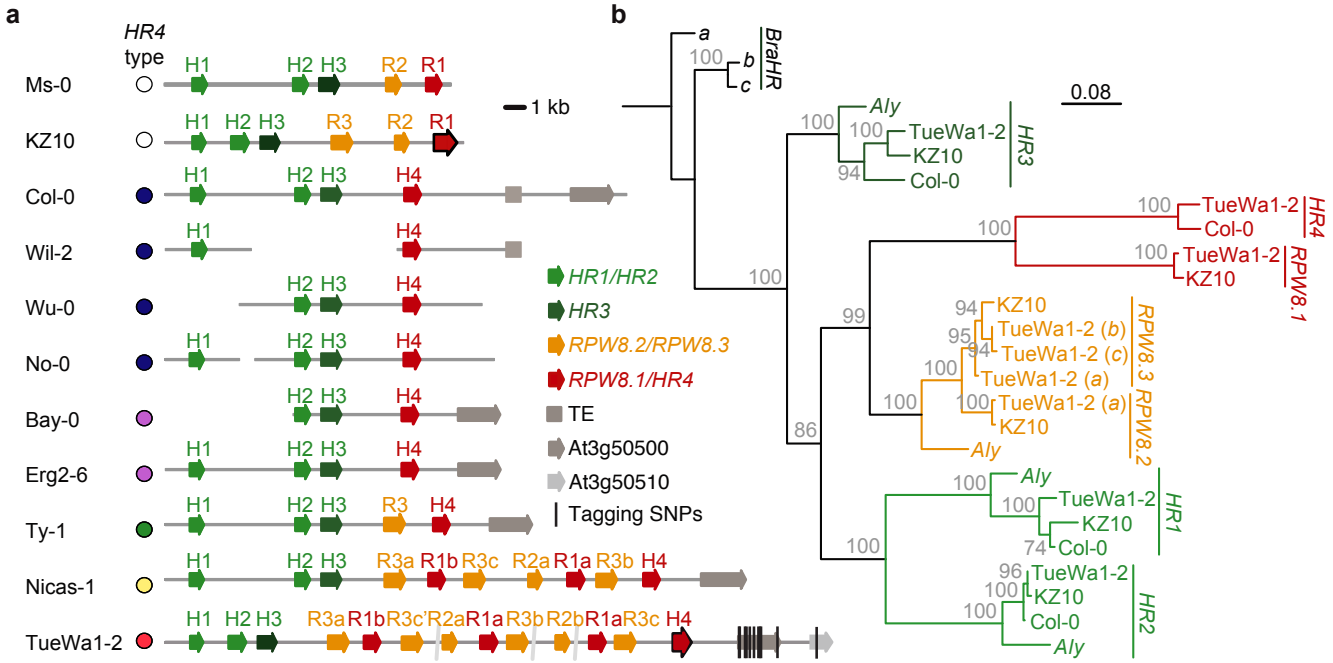

Figure 4. Structural variation of the *RPW8/HR* cluster
(**a**) The *RPW8/HR* cluster in different accessions. Gaps in the TueWa1-2 assembly are indicated. Color coding of *HR4* alleles according to Figure 6. Tagging SNPs found in GWAS marked in TueWa1-2 *RPW8/HR* cluster as black vertical lines. (**b**) Maximum likelihood tree of *RPW8/HR* genes from three *A. thaliana* accessions and the *A. lyrata* and *B. rapa* reference genomes. Branch lengths in nucleotide substitutions are indicated. Bootstrap values (out of 100) are indicated on each branch. Note the long branches of the *HR4/RPW8.1* clade.

Causality of RPW8/HR C-terminal repeats

To further narrow down the mutations that cause autoimmunity, we compared *RPW8.1*^{KZ10} and *HR4*$^{Fei-0}$ with other *RPW8/HR* alleles from global *A. thaliana* samples [62]. Some *RPW8.1* alleles have intragenic duplications of a sequence encoding a 21-amino acid repeat of unknown function (QWDDIKEIKAKISEMDTKLA[D/E]) at the C-terminal end of the protein [45]. In HR4, there is a related 14-amino acid repeat (IQV[H/D]QW[T/I]DIKEMKA). Both RPW8.1 and HR4 repeats are predicted to fold into extended alpha-helices, but only the RPW8.1 repeats appear to have the potential to form coiled coils [63].

In the hybrid necrosis risk allele *RPW8.1*^{KZ10}, there are two complete and one partial repeat, while the non-risk allele *RPW8.1*$^{Ms-0}$ has only one repeat (**Figure 5a**). To experimentally test the effect of repeat number variation and other polymorphisms, we generated a series of derivatives in which we altered the number of repeats and swapped different portions of the coding sequences between the *RPW8.1*^{KZ10} risk and *RPW8.1*$^{Ms-0}$ non-risk alleles, and between the *HR4*$^{Fei-0}$ and *HR4*^{ICE106} risk and the *HR4*$^{Col-0}$ non-risk alleles (**Figure 5a**). We first confirmed that a 1.4 kb promoter fragment of *RPW8.1*^{KZ10} and a 1.2 kb promoter fragment of *HR4*$^{Fei-0}$ in combination with coding sequences of risk alleles were sufficient to induce hybrid necrosis (**Figure 3c and**

Figure 5a, b). To simplify discussion of the chimeras, the N-terminal portion was labeled with the initial of the accession in italics ("*M*", "*K*", etc.), complete repeats were labeled with regular capital letters ("A", "B", etc.), the partial repeat in KZ10 with a lowercase letter ("c"), and the C-terminal tails with Greek letters ("α", "β", etc.). Fragments with identical amino acid sequence have the same letter designation.

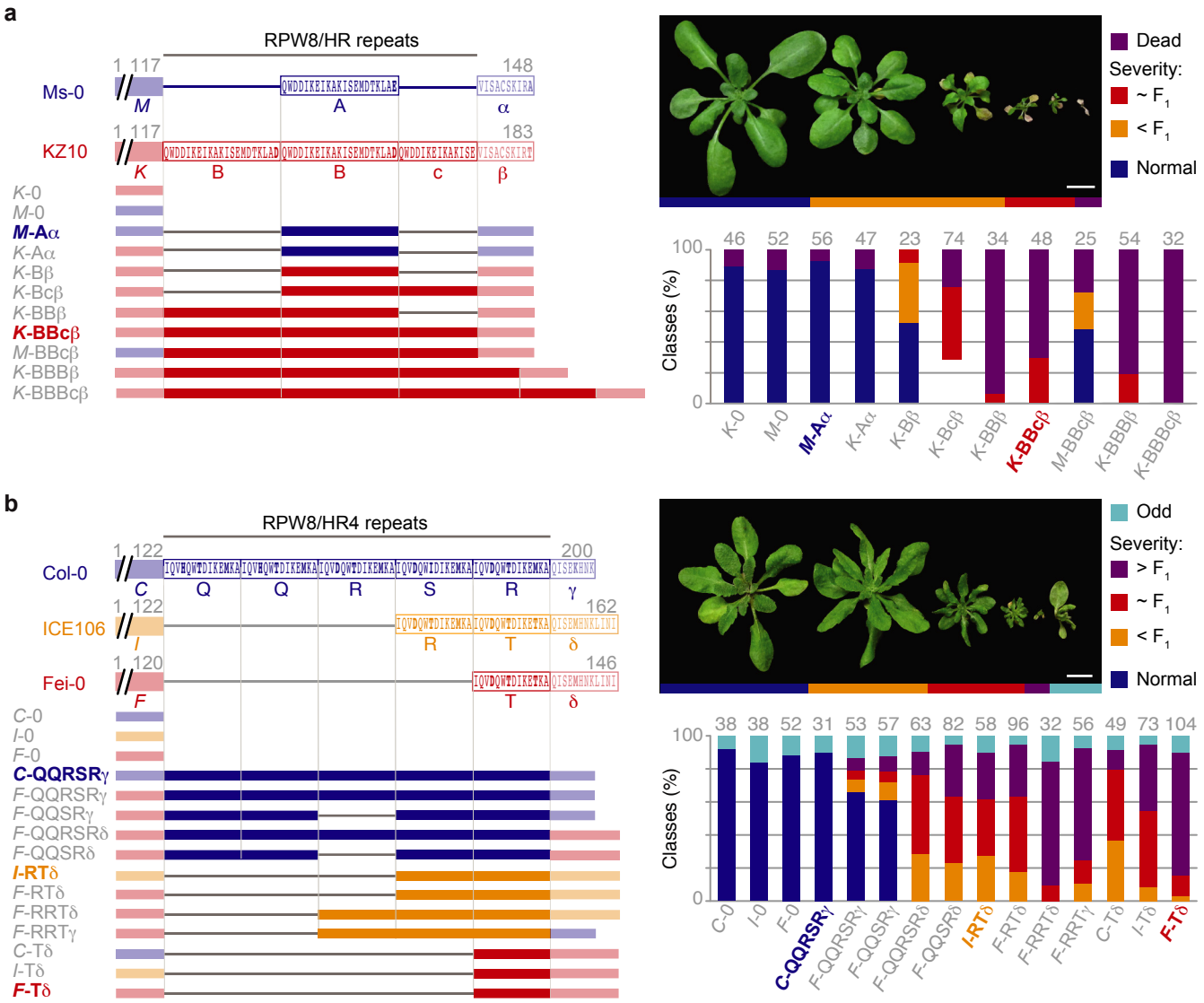

Figure 5. Necrosis-inducing activity of *RPW8.1* and *HR4* chimeras

N-terminal portions indicated with the initial of the accession in italics ("*K*", "*M*", etc.), complete repeats indicated with regular capital letters ("A", "B", etc.), the partial repeat in KZ10 with a lowercase letter ("c"), and the C-terminal tails with Greek letters ("α", "β", etc.). Non-repeat portions are semi-transparent. Repeats with identical amino acid sequences have the same letter designation. Numbers indicate amino acid positions. Constructs on the left, and distribution across phenotypic classes in T_1 transformants on the right, with *n* given on top of each column. Natural alleles labeled in color and bold. (**a**) *RPW8.1* chimeras, driven by the *RPW8.1*^{KZ10} promoter, were introduced into Mrk-0, which carries the corresponding incompatible *RPP7* allele. (**b**) *HR4* chimeras, driven by the *HR4*$^{Fei-0}$ promoter, were introduced into Lerik1-3, which carries the corresponding incompatible *RPP7* allele. Scale bars indicate 1 cm.

Modifying the number of repeats in *RPW8.1* affected the frequency and severity of necrosis in T_1 plants in a Mrk-0 background dramatically. In the case of *RPW8.1*^{KZ10}, deletion of the first full repeat ("*K*-Bcβ", with the KZ10 configuration being "*K*-BBcβ") substantially reduced the number of plants that died in the first three weeks of growth. Additional deletion of the partial repeat ("*K*-Bβ") reduced death and necrosis even further (**Figure 5a**). In contrast, the extension of the partial repeat ("*K*-BBBβ") or addition of a full repeat ("*K*-BBBcβ") increased the necrosis-inducing activity of *RPW8.1*, such that almost all T_1 plants died without making any true leaves. However, it appears that not all repeats function equally, as removal of the partial repeat slightly increased necrosis-inducing activity ("*K*-BBβ"). Polymorphisms in the N-terminal non-repeat region seemed to contribute to necrosis, as swaps of the N-terminal Ms-0 fragment ("*M*-BBcβ" or "*M*-BBBβ") induced weaker phenotypes than the corresponding variants with the N-terminal fragment from KZ10. Nevertheless, we note that the normal KZ10 repeat configuration was sufficient to impart substantial necrosis-inducing activity on a chimera in which the N-terminal half was from Ms-0, which is distinguished from KZ10 by nine nonsynonymous substitutions outside the repeats.

Different from the RPW8.1 situation, the relationship between HR4 repeat length and necrosis-inducing activity is more complex. The natural alleles suggested a negative correlation of repeat number with necrosis-inducing activity when crossed to Lerik1-3, since the non-risk HR4 allele from Col-0 has five full repeats, while weak risk alleles such as the one from ICE106 have two, and the strong risk allele from Fei-0 has only one (**Figure 5b**). Addition of a full repeat to HR4^{Fei-0} ("*F*-RTδ", with the original Fei-0 configuration being "*F*-Tδ") reduced its activity to a level similar to that of HR4^{ICE106} ("*I*-RTδ"). These experiments also showed that *HR4* sequences from Fei-0 and ICE106, which are distinguished by four non-synonymous changes outside the repeats, are largely interchangeable. Deletion of a full repeat from HR4^{ICE106} ("*I*-Tδ") modestly increased HR4 activity (**Figure 5b**). Together, the chimera analyses indicated that the quantitative differences between crosses of Fei-0 and ICE106 to Lerik1-3 (**Figure 1 and S2**) are largely due to variation in HR4 repeat number. This is further supported by the necrosis-inducing activity of a chimera in which the repeats in the Col-0 non-risk allele were replaced with those from *HR4*$^{Fei-0}$ ("*C*-Tδ", with the original Col-0 configuration being "*C*-QQRSRγ") (**Figure 5b and S4**).

However, repeat number alone is not the only determinant of necrosis-inducing activity of *HR4* in combination with *RPP7*$^{Lerik1-3}$. Adding another repeat to the "*F*-RTδ" chimera, resulting in "*F*-RRTδ", increased the activity of *HR4*$^{Fei-0}$ again, perhaps suggesting that there is an optimal length for *HR4* to interact with *RPP7*$^{Lerik1-3}$.

Unlike RPW8.1, the C-terminal tails of HR4 proteins beyond the RPW8/HR repeats (fragments "γ" and "δ") differ in length between necrosis-risk and non-risk variants (**Figure 5b**). Swapping only these two fragments affected HR4 activity substantially, and converted two chimeras with weak necrosis-inducing activity

("*F*-QQRSRγ" to "*F*-QQRSRδ" and "*F*-QQSRγ" to "*F*-QQSRδ") into chimeras with activity resembling that of HR4^{ICE106} (which is "*I*-RTδ").

Taken together, the swap experiments lead us to conclude that naturally occurring variation in the configuration of RPW8/HR repeats as well as the short C-terminal tail play a major role in quantitatively modulating the severity of autoimmune phenotypes when *RPW8/HR* variants are combined with *RPP7* alleles from Mrk-0 and Lerik1-3.

Prediction of *RPP7*-dependent hybrid performance using *RPW8.1/HR4* haplotypes

To obtain a better picture of *RPW8.1/HR4* variation, we remapped the raw reads from the 1001 Genomes project (http://1001genomes.org) to the longest *RPW8.1* and *HR4* alleles, *RPW8.1*^{KZ10} and *HR4*$^{Col-0}$, as references. We inferred presence of either allele when a fraction of each gene that corresponded to the shortest allele confirmed by Sanger sequencing to carry *RPW8.1* or *HR4* was covered by reads (**Table S4 and S5**). The results suggested that *HR4*-carrying accessions are more rare than those carrying RPW8.1 alleles (285 vs. 903 out of 1,221 accessions). The short, necrosis-linked *HR4* risk alleles (**Figure 6a, Type 6, red**, **Type 5, yellow**) were predicted to be as frequent as the long non-risk variants (**Figure 6a, Type 1-4, Figure 6b and Table S4**), whereas for *RPW8.1*, only seven accessions were predicted to have the long *RPW8.1*^{KZ10}-type risk variant (**Figure 6a, Type 1 pink and Table S5**).

To confirm the short read-based length predictions, *RPW8.1* was PCR amplified from 28 accessions and *HR4* from 113 accessions (**Table S4, S5** and **Figure 6a-d**). The *RPW8.1/HR4* lengths determined by Sanger sequencing of PCR products indicated approximately 95% accuracy in distinguishing between long and short variants by Illumina read mapping (**Figure S5**, **Table S4 and S5**). We found new variants with different arrangements of *HR4* repeats, but none were as short as *HR4*$^{Fei-0}$ or *HR4*^{ICE106} (**Figure 6a, b**). The short *HR4* variants are found across much of the global range of *A. thaliana* (**Figure 6c**), whereas the much rarer *RPW8.1*^{KZ10}-like variant was exclusive to Central Asia. We also observed that sequences of the two short *HR4* types, associated with hybrid necrosis, were more conserved than the longer ones, each of the short types belonging to only one haplotype compared to long *HR4* alleles, which belonged to multiple haplotypes (**Figure 6d**).

The extensive information on *RPW8.1/HR4* haplotypes allowed us to use test crosses to determine whether interaction with either *RPP7*$^{Mrk-0}$ or *RPP7*$^{Lerik1-3}$ is predictable from sequence, specifically from repeat number (**Figure 6e, f**). As expected, accessions with the longest Type 1, KZ10-like *RPW8.1* alleles (**Figure 6e, pink**) produced necrotic hybrid progeny when crossed to Mrk-0, whereas accessions carrying the two shorter Type 2 and 3 *RPW8.1* alleles did not (**Figure 6e, green, brown Table S7**). The situation was similar for *HR4*; all tested accessions but two with the shortest, *HR4*$^{Fei-0}$-like alleles (**Figure 6f, red**) produced strongly necrotic progeny when crossed to Lerik1-3, while accessions carrying the second shortest, *HR4*^{ICE106}-like alleles (**Figure 6f**, **Type 5, yellow, Table S6**) produced more mildly affected progeny. Hybrid progeny of Lerik1-3 and

accessions carrying other *HR4* alleles did not show any signs of necrosis (**Figure 6f**). Necrosis was correlated with reduction in overall size of plants, which in turn correlates with RPW8.1/HR4 repeat length (**Figure 6g** and **Table S8**). Finally, *HR4*$^{Fei-0}$-like alleles in two accessions caused a mild phenotype similar to *HR4*^{ICE106}, suggesting the presence of genetic modifiers that partially suppress autoimmune symptoms.

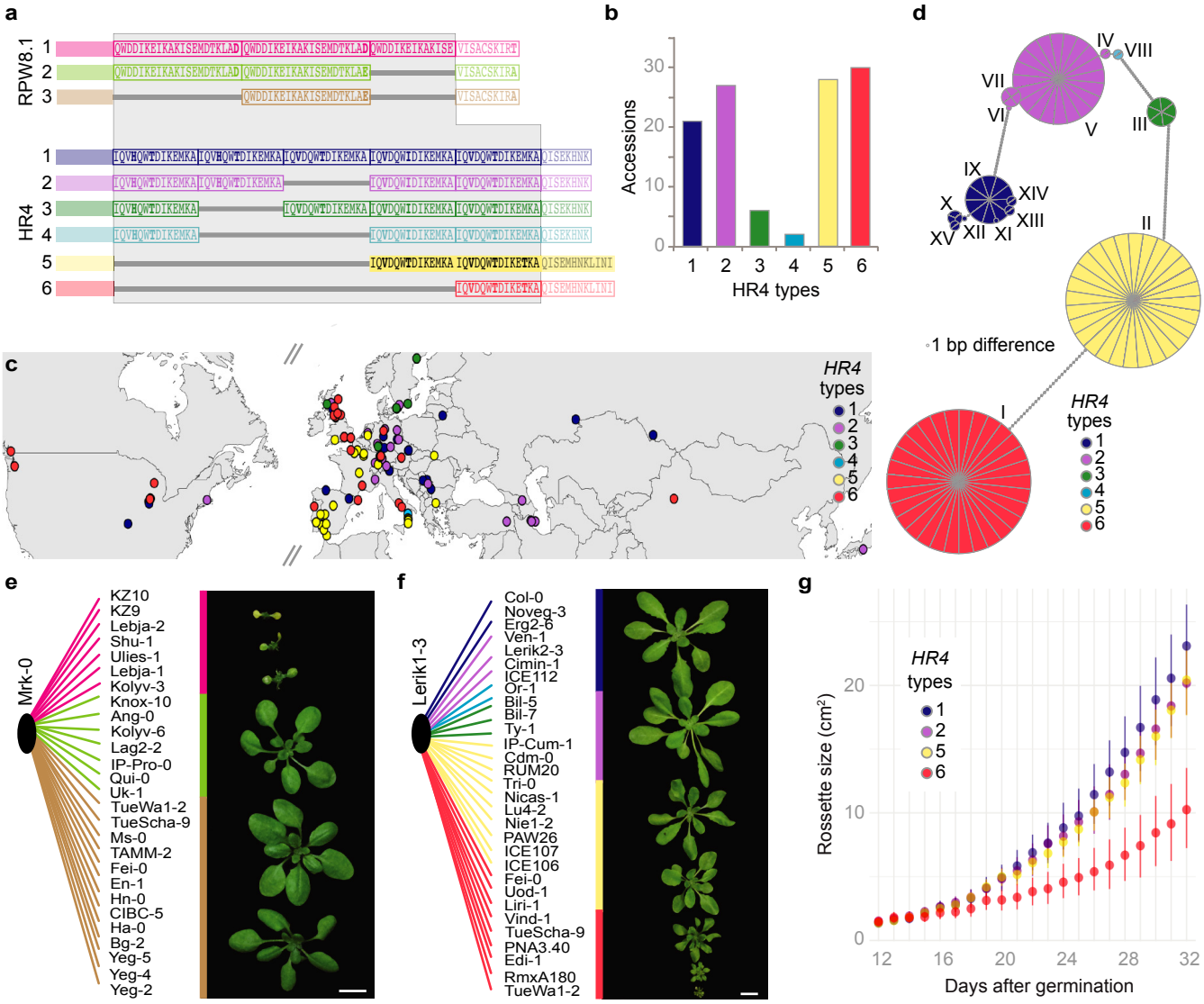

Figure 6. Sequence variation of a large collection of *RPW8.1* and *HR4* alleles
(**a**) Repeat polymorphisms in RPW8.1 and HR4 proteins (grey background). N-terminal regions and tails are semi-transparent. (**b**) Distribution of *HR4* types across 113 Sanger sequenced alleles (see Table S4). (**c**) Distribution of *HR4* allele types in Eurasia and North America. (**d**) Haplotype network of *HR4* alleles, with a 1-bp minimum difference. (**e**) F_1 progeny of Mrk-0 crossed to accessions with different *RPW8.1* alleles. Short *RPW8.1* variants do not induce hybrid necrosis. (**f**) F_1 progeny of Lerik1-3 crossed to accessions with different *HR4* alleles. The shortest *HR4* alleles (red) cause strong hybrid necrosis, the second shortest *HR4* alleles (yellow) cause mild hybrid necrosis. (**g**) Rosette growth of F_1 progeny from Lerik1-3 and accessions carrying different *HR4* alleles. The shortest *HR4* allele causes a strong growth reduction, while the second-shortest *HR4* allele has a milder effect. Scale bars indicate 1 cm.

Discussion

Being able to predict hybrid performance – both whether hybrids are better or worse than their parents – is highly valuable in plant breeding. While heterosis or hybrid vigor are desirable, hybrid weakness, with hybrid necrosis being one prominent example among many [12,64], must be avoided. Most, but not all, previously identified hybrid necrosis loci in *A. thaliana* seem rare [20,22,65]. It is not only noteworthy that some of the *RPW8/HR* alleles studied here are sufficiently common to be identifiable by GWAS, but also that a relatively simple measure of variation – length of the RPW8/HR repeats – can be predictive of their interaction with different *RPP7* hybrid necrosis-risk alleles. Such findings are of interest in plant breeding, as predictable hybrid incompatibilities can guide the designs of hybridization panels.

Allelic interactions between *RPW8/HR* and *RPP7*

The *RPW8/HR* cluster is remarkably variable in terms of copy number, reminiscent of many multi-gene clusters carrying NLR-type *R* genes [26,33,66]. While the first three genes in the cluster, *HR1*, *HR2* and *HR3*, are generally well conserved, there is tremendous variation in the *HR4* and *RPW8.1* genes, which are specific to the *A. thaliana* lineage, as well as in the *RPW8.2* and *RPW8.3* genes. Focusing on the *RPW8.2/RPW8.1/HR4* clade, their copy number ranges from one in Col-0 to at least ten in TueWa1-2 (which is very similar to Fei-0 based on PCR survey data) (**Figure 4a**). We have not found accessions carrying necrosis-risk type alleles at both *RPW8.1* and *HR4* (**Tables S4 and S5**). This is likely because of reduced recombination between *HR4* and *RPW8.1*, although it is also consistent with there being limits to reconfiguration of immune alleles, to reduce the risks of potentially fatal interactions within the immune system [20,67]. This may be especially true for the interaction with *RPP7*, an NLR cluster with extreme variation [55,56]. We attempted to find evidence for potential linkage between specific *RPW8/HR* alleles and *RPP7* alleles, but the poor annotation of polymorphisms in the 1001 Genomes project due to structural variation at both loci made such analyses difficult. Nevertheless, that the *HR4* hybrid necrosis-risk allele is not rare and widely distributed, accounting for half of all *HR4* carriers (**Figure 6b, c**), suggests that it might provide adaptive benefits, as postulated before for *ACD6* hybrid necrosis-risk alleles [22].

That there are three different allelic pairs at the two clusters that cause hybrid necrosis strongly supports a rather direct connection between RPW8/HR and RPP7 proteins. The C-terminal portion of RPW8/HR proteins appears to have a regulatory role, demonstrated by our chimera studies and also inferred from interaction with a regulatory 14-3-3 protein [68], making the RPW8/HR repeats and the C-terminal tail a possible target for pathogen effectors. At least some RPP7 proteins might act as guards for RPW8/HR proteins and sense their modification by pathogen effectors [26,69]. Despite the extensive structural variation at *RPP7* [56], the only confirmed recognition specificity of the locus is for *Hpa* strain Hiks1 in *A. thaliana* accession Col-0 [55,59]. Inactivation of *HR4* did not compromise $RPP7^{Col\text{-}0}$ mediated resistance to Hiks1, which could be

interpreted in several different ways. For example, *RPP7*$^{Col-0}$ might guard a protein different from HR4 or there might be redundancy among HR proteins; interaction of NLR homologs with sequence unrelated proteins is not without precedence [25,26,70].

Similarity of RPW8/HR to fungal and mammalian immune proteins

RPW8.1 and *RPW8.2* genes can confer resistance to filamentous pathogens [43,71], while the function of *HR4* is unclear. That *HR4* is highly induced upon biotic stresses and in autoimmune hybrids [15,44,72], and that HR proteins similar to RPW8 proteins localize to extrahaustorial membranes of infected plants [73], all point to similar biochemical roles of RPW8 and HR proteins. The N-terminal portion of RPW8 and HR proteins can be homology modeled on a multi-helix bundle in the animal MLKL protein [50]. This multi-helix bundle can insert into the cell membrane, thereby disrupting membrane integrity and triggering cell death. The insertion is regulated by a helix that follows immediately the multi-helix bundle [74–78]. It is tempting to speculate that the RPW8/HR repeats and the C-terminal tail, which together make up the C-terminal portions of the proteins, similarly regulate activity of RPW8.1 and HR4. A positive regulator of RPW8-mediated disease resistance, a 14-3-3 protein, interacts specifically with the C-terminal portion of RPW8.2, consistent with this part of the protein controlling RPW8/HR activity [68]. However, different from MLKL, removal of the portion equivalent to helix 6 in MLKL does not make RPW8.1 or HR4 autoactive (**Figure 5**). This is consistent with extensive mutant analyses of RPW8.2, which identified the C-terminal portion as preventing targeting to the extrahaustorial membrane in the presence of a fungal pathogen, and instead directing the truncated proteins to the nucleus [79].

Can we conclude from the MLKL homology that RPW8 and HR proteins form similar pores as MLKL? Unfortunately, this is not immediately obvious, as a different mechanism has been suggested for fungal HET-S and HELLP proteins, whose HeLo and HeLo-like (HELL) domains are similar to the MLKL/RPW8/HR shared domain [51–53]. In this case, however, it has been suggested that the multi-helix bundle regulates the ability of an N-terminal transmembrane domain to insert into the membrane, which in turn also disrupts membrane integrity [52]. Thus, it is unclear whether the potential multi-helix bundle of RPW8/HR proteins can insert into the membrane.

The fungal *HET-S* locus, which – intriguingly – is involved in a type of non-self recognition called heterokaryon incompatibility [80], is located next to *NWD2*, which encodes an NLR protein that regulates the pore-forming activity of HET-S [81]. This is reminiscent of the interaction between RPW8/HR proteins and the NLR protein RPP7. Adjacent HeLo-/HELL-domain encoding genes and NLR genes are found in many fungal genomes [82–85]. In addition, the mammalian NLR protein NLRP3 and its adaptor protein ASC interact in a very similar manner as HET-S and NWD2 do [86]. A split two-component system consisting of an NLR (NWD2 homologs in fungi, NLRP3 in mammals, and RPP7 proteins in plants) and a cell death executor (HeLo/HELL domain proteins in fungi, ASC in mammals, and RPW8/HR proteins in plants) thus appears to be

an evolutionarily conserved or convergent module for activating innate immunity. What this exactly implies for RPW8/HR and RPP7 activation is unclear, but one possibility is that in this system, both components activate cell death. In analogy with the fungal and mammalian situation, RPP7-regulated RPW8/HR proteins might directly induce cell death at the cell membrane. Different from fungi and mammals, RPW8/HR-regulated RPP7 proteins may in addition indirectly induce cell death through conventional NLR signaling.

Conclusions

In summary, we have described in detail an intriguing case of hybrid necrosis in *A. thaliana*, where three different pairs of alleles at a conventional complex NLR resistance gene cluster, *RPP7*, and alleles at another complex, but non-NLR resistance gene cluster, *RPW8/HR*, interact to trigger autoimmunity in the absence of pathogens. This finding suggests that conflict does not occur randomly among different components of the immune system, but that certain pairs of loci are more likely to misbehave than others. Finally, that the *RPW8/HR* cluster has been genetically linked to broad-spectrum disease resistance, while *RPP7* confers race-specific resistance, provides yet another link between different arms of the plant immune system [87].

Materials and Methods

Plant material

Stock numbers of accessions used are listed in Table S4-S5. All plants were stratified in the dark at 4°C for 4-6 days prior to planting on soil. Late flowering accessions were vernalized for six weeks under short day conditions (8 h light) at 4°C as seedlings. All plants were grown in long days (16 h light) at 16°C or 23°C at 65% relative humidity under Cool White fluorescent light of 125 to 175 µmol m^{-2} s^{-1}. Transgenic seeds were selected either with 1% BASTA (Sigma-Aldrich), or by mCherry fluorescence [88]. Constructs are listed in Table S11.

Genotyping by Sequencing and QTL mapping

Genomic DNA was isolated from Lerik1-3 x ICE106/ICE107 F_2 and F_3 individuals and from ICE79 x Don-0 F_2 individuals using a BioSprint 96 instrument and the BioSprint 96 DNA Plant Kit (Qiagen, Hilden, Germany). The individuals represented all classes of segregating phenotypes. Genotyping-by-Sequencing (GBS) using RAD-seq was used to genotype individuals in the mapping populations with *Kpn*I tags [57]. Libraries were single-end sequenced on a HiSeq 3000 instrument (Illumina, San Diego, USA) with 150 bp reads. Reads were processed with SHORE [89] and mapping was performed with BWA/MEM to the *A. thaliana* Col-0 reference genome [90]. QTL was performed using R/qtl with the information from 330 individuals and 2,989 markers for the Lerik1-3 x ICE106/107 populations, and 304 individuals and 2,207 markers for the ICE79 x Don-0 population.

GWAS

Lerik1-3-dependent hybrid necrosis in F_1 progeny from crosses with 80 accessions [91] was scored as 1 or 0. The binary trait with accession information was submitted to the easyGWAS platform [58], the FaSTLMM algorithm was chosen [92]. A $-\log_{10}$(p-value) was calculated for every SNP along the five *A. thaliana* chromosomes.

RPW8.1/HR4 length prediction

Short reads from the 1001 Genomes project (http://1001genomes.org) were mapped using GenomeMapper [93] as implemented in SHORE [89] allowing 5 mismatches per read. Sequences of the *RPW8/HR* clusters from Col-0 and KZ10 were provided as references and the covered region for *RPW8.1*^{KZ10} and *HR4*$^{Col-0}$ was retrieved.

RPW8.1/HR4 sequence analysis

Overlapping fragments covering the *HR4/RPW8.1* genomic region were PCR amplified from Fei-0 (oligonucleotides are listed in table S10). Fragments were cloned into pGEM®-T Easy (Promega, Madison, WI, USA) and Sanger sequenced. Sequences were assembled using Seqman (DNAStar Inc., Madison, WI, USA), visualized with Gene Construction Kit (Textco BioSoftware, Raleigh, NC, USA), and Aligned with Aliview using MUSCLE [94]. A maximum-likelihood tree for *RPW8/HR* genes (coding portions of exons and introns) was computed using RaxML [95] and visualized with Figtree.

Population genetics

The geographical distribution of the 113 accessions carrying different *HR4* alleles was plotted using R (version 0.99.903). Packages maps, mapdata, mapplots and scales were used. A haplotype network was built using a cDNA alignment of 113 *HR4* alleles from different accessions. The R packages used were ape (dist.dna function) and pegas (haploNet function).

Histology

Cotyledons from 18 day-old seedlings were collected and 1 ml of lactophenol Trypan Blue solution (20 mg Trypan Blue, 10 g phenol, 10 ml lactic acid, 10 ml glycerol and 10 ml water) diluted 1 : 2 in 96% ethanol was added for 1 hour at 70°C. Trypan Blue was removed, followed by the addition of 1 ml 2.5g/ml chloral hydrate and overnight incubation. The following day, the de-stained cotyledons were transferred to 50% glycerol and mounted on slides.

Oligonucleotides

See Table S10.

Author contributions

CB, DW, EC conceived and designed the study, CB, RW, AH, WX, MZ, WWHH, EC performed the experiments, CB, STK, JH, ALVdW, IB, GW, EC analyzed the results, and CB, DW, EC wrote the paper.

Competing interests. The authors have declared that no competing interests exist.

Acknowledgements

We thank Jane Parker for the *H. arabidopsidis* Hiks1 isolate, Katrin Fritschi and Camilla Kleinhempel for technical support, Gautam Shirsekar for help with the pathology assays and discussions, and Christian Kubica for help with visualization of PacBio sequence data. Supported by a Marie Curie postdoctoral fellowship (2014-655295 to RW), an Academic Research Fund (R-154-000-B33-114) from the National University of Singapore (EC), and ERC Advanced Grant IMMUNEMESIS (340602), the DFG through Collaborative Research Center CRC1101, and the Max Planck Society (DW).

Bibliography

1. Duvick DN. The Contribution of Breeding to Yield Advances in maize (Zea mays L.). Advances in Agronomy. Academic Press; 2005. pp. 83–145.
2. Wang Y, Xue Y, Li J. Towards molecular breeding and improvement of rice in China. Trends Plant Sci. 2005;10: 610–614.
3. Hanušová R, Hsam SLK, Bartoš P, Zeller FJ. Suppression of powdery mildew resistance gene Pm8 in Triticum aestivum L. (common wheat) cultivars carrying wheat-rye tranlocation T1BL·1RS. Heredity . The Genetical Society of Great Britain; 1996;77: 383.
4. Nelson JC, Singh RP, Autrique JE, Sorrells ME. Mapping genes conferring and suppressing leaf rust resistance in wheat. Crop Sci. Crop Science Society of America; 1997;37: 1928–1936.
5. Knott DR. Inheritance of Resistance to Stem Rust in Medea Durum Wheat and the Role of Suppressors. Crop Sci. 2000;40. doi:10.2135/cropsci2000.40198x
6. McIntosh RA, Zhang P, Cowger C, Parks R, Lagudah ES, Hoxha S. Rye-derived powdery mildew resistance gene Pm8 in wheat is suppressed by the Pm3 locus. Theor Appl Genet. 2011;123: 359–367.
7. Chen W, Liu T, Gao L. Suppression of stripe rust and leaf rust resistances in interspecific crosses of wheat. Euphytica. 2013;192: 339–346.
8. Liu W, Danilova TV, Rouse MN, Bowden RL, Friebe B, Gill BS, et al. Development and characterization of a compensating wheat-Thinopyrum intermedium Robertsonian translocation with Sr44 resistance to stem rust (Ug99). Theor Appl Genet. 2013;126: 1167–1177.

9. Stirnweis D, Milani SD, Brunner S, Herren G, Buchmann G, Peditto D, et al. Suppression among alleles encoding nucleotide-binding-leucine-rich repeat resistance proteins interferes with resistance in F1 hybrid and allele-pyramided wheat plants. Plant J. 2014;79: 893–903.
10. Hurni S, Brunner S, Stirnweis D, Herren G, Peditto D, McIntosh RA, et al. The powdery mildew resistance gene Pm8 derived from rye is suppressed by its wheat ortholog Pm3. Plant J. 2014;79: 904–913.
11. Bomblies K, Weigel D. Hybrid necrosis: autoimmunity as a potential gene-flow barrier in plant species. Nat Rev Genet. 2007;8: 382–393.
12. Vaid N, Laitinen RAE. Diverse paths to hybrid incompatibility in Arabidopsis. Plant J. 2019;97: 199–213.
13. Chen C, Zhiguo E, Lin H-X. Evolution and Molecular Control of Hybrid Incompatibility in Plants. Front Plant Sci. 2016;7: 1135.
14. Krüger J, Thomas CM, Golstein C, Dixon MS, Smoker M, Tang S, et al. A tomato cysteine protease required for Cf-2-dependent disease resistance and suppression of autonecrosis. Science. 2002;296: 744–747.
15. Bomblies K, Lempe J, Epple P, Warthmann N, Lanz C, Dangl JL, et al. Autoimmune response as a mechanism for a Dobzhansky-Muller-type incompatibility syndrome in plants. PLoS Biol. 2007;5: e236.
16. Jeuken MJW, Zhang NW, McHale LK, Pelgrom K, den Boer E, Lindhout P, et al. Rin4 causes hybrid necrosis and race-specific resistance in an interspecific lettuce hybrid. Plant Cell. 2009;21: 3368–3378.
17. Alcázar R, García AV, Parker JE, Reymond M. Incremental steps toward incompatibility revealed by Arabidopsis epistatic interactions modulating salicylic acid pathway activation. Proceedings of the National Academy of Sciences. 2009;106: 334–339.
18. Alcázar R, García AV, Kronholm I, de Meaux J, Koornneef M, Parker JE, et al. Natural variation at Strubbelig Receptor Kinase 3 drives immune-triggered incompatibilities between Arabidopsis thaliana accessions. Nat Genet. 2010;42: 1135–1139.
19. Yamamoto E, Takashi T, Morinaka Y, Lin S, Wu J, Matsumoto T, et al. Gain of deleterious function causes an autoimmune response and Bateson-Dobzhansky-Muller incompatibility in rice. Mol Genet Genomics. 2010;283: 305–315.
20. Chae E, Bomblies K, Kim S-T, Karelina D, Zaidem M, Ossowski S, et al. Species-wide genetic incompatibility analysis identifies immune genes as hot spots of deleterious epistasis. Cell. 2014;159: 1341–1351.
21. Chen C, Chen H, Lin Y-S, Shen J-B, Shan J-X, Qi P, et al. A two-locus interaction causes interspecific hybrid weakness in rice. Nat Commun. 2014;5: 3357.
22. Todesco M, Kim ST, Chae E, Bomblies K, Zaidem M, Smith LM, et al. Activation of the Arabidopsis thaliana immune system by combinations of common ACD6 alleles. PLoS Genet. 2014;10: e1004459.
23. Sicard A, Kappel C, Josephs EB, Lee YW, Marona C, Stinchcombe JR, et al. Divergent sorting of a balanced ancestral polymorphism underlies the establishment of gene-flow barriers in Capsella. Nat Commun.

2015;6: 7960.

24. Cesari S. Multiple strategies for pathogen perception by plant immune receptors. New Phytol. 2017; doi:10.1111/nph.14877
25. Zhang X, Dodds PN, Bernoux M. What Do We Know About NOD-Like Receptors in Plant Immunity? Annu Rev Phytopathol. 2017;55: 205–229.
26. Monteiro F, Nishimura MT. Structural, Functional, and Genomic Diversity of Plant NLR Proteins: An Evolved Resource for Rational Engineering of Plant Immunity. Annu Rev Phytopathol. 2018;56: 243–267.
27. Kourelis J, van der Hoorn RAL. Defended to the Nines: 25 years of Resistance Gene Cloning Identifies Nine Mechanisms for R Protein Function. Plant Cell. American Society of Plant Biologists; 2018; doi:10.1105/tpc.17.00579
28. Karasov TL, Horton MW, Bergelson J. Genomic variability as a driver of plant-pathogen coevolution? Curr Opin Plant Biol. 2014;18: 24–30.
29. Jacob F, Vernaldi S, Maekawa T. Evolution and Conservation of Plant NLR Functions. Front Immunol. 2013;4: 297.
30. Gos G, Slotte T, Wright SI. Signatures of balancing selection are maintained at disease resistance loci following mating system evolution and a population bottleneck in the genus Capsella. BMC Evol Biol. 2012;12: 152.
31. Nagy ED, Bennetzen JL. Pathogen corruption and site-directed recombination at a plant disease resistance gene cluster. Genome Res. 2008;18: 1918–1923.
32. Wicker T, Yahiaoui N, Keller B. Illegitimate recombination is a major evolutionary mechanism for initiating size variation in plant resistance genes. Plant J. 2007;51: 631–641.
33. Baggs E, Dagdas G, Krasileva KV. NLR diversity, helpers and integrated domains: making sense of the NLR IDentity. Curr Opin Plant Biol. 2017;38: 59–67.
34. Lemons D, McGinnis W. Genomic evolution of Hox gene clusters. Science. 2006;313: 1918–1922.
35. Zeng G, Zhang P, Zhang Q, Zhao H, Li Z, Zhang X, et al. Duplication of a Pks gene cluster and subsequent functional diversification facilitate environmental adaptation in Metarhizium species. PLoS Genet. 2018;14: e1007472.
36. Trowsdale J. The gentle art of gene arrangement: the meaning of gene clusters. Genome Biol. 2002;3: COMMENT2002.
37. Olukolu BA, Wang G-F, Vontimitta V, Venkata BP, Marla S, Ji J, et al. A Genome-Wide Association Study of the Maize Hypersensitive Defense Response Identifies Genes That Cluster in Related Pathways. PLoS Genet. Public Library of Science; 2014;10: e1004562.
38. Wu C-H, Abd-El-Haliem A, Bozkurt TO, Belhaj K, Terauchi R, Vossen JH, et al. NLR network mediates immunity to diverse plant pathogens. Proc Natl Acad Sci U S A. National Academy of Sciences; 2017;114: 8113–8118.

39. Wu Z, Li M, Dong OX, Xia S, Liang W, Bao Y, et al. Differential regulation of TNL-mediated immune signaling by redundant helper CNLs. New Phytol. 2018; doi:10.1111/nph.15665
40. Castel B, Ngou P-M, Cevik V, Redkar A, Kim D-S, Yang Y, et al. Diverse NLR immune receptors activate defence via the RPW8-NLR NRG1. New Phytol. 2018; doi:10.1111/nph.15659
41. Qi T, Seong K, Thomazella DPT, Kim JR, Pham J, Seo E, et al. NRG1 functions downstream of EDS1 to regulate TIR-NLR-mediated plant immunity in Nicotiana benthamiana. Proc Natl Acad Sci U S A. 2018;115: E10979–E10987.
42. Zhang Y, Xia R, Kuang H, Meyers BC. The Diversification of Plant NBS-LRR Defense Genes Directs the Evolution of MicroRNAs That Target Them. Mol Biol Evol. 2016;33: 2692–2705.
43. Xiao S, Ellwood S, Calis O, Patrick E, Li T, Coleman M, et al. Broad-spectrum mildew resistance in Arabidopsis thaliana mediated by RPW8. Science. 2001;291: 118–120.
44. Xiao S, Emerson B, Ratanasut K, Patrick E, O'Neill C, Bancroft I, et al. Origin and maintenance of a broad-spectrum disease resistance locus in Arabidopsis. Mol Biol Evol. 2004;21: 1661–1672.
45. Orgil U, Araki H, Tangchaiburana S, Berkey R, Xiao S. Intraspecific genetic variations, fitness cost and benefit of RPW8, a disease resistance locus in Arabidopsis thaliana. Genetics. 2007;176: 2317–2333.
46. El Kasmi F, Nishimura MT. Structural insights into plant NLR immune receptor function. Proc Natl Acad Sci U S A. 2016;113: 12619–12621.
47. Wróblewski T, Spiridon L, Martin EC, Petrescu A-J, Cavanaugh K, Jose-Truco M, et al. Genome-wide functional analyses of plant coiled-coil NLR-type pathogen receptors reveal essential roles of their N-terminal domain in oligomerization, networking, and immunity. PLoS Biol. 2018;16: e2005821.
48. Collier SM, Hamel L-P, Moffett P. Cell death mediated by the N-terminal domains of a unique and highly conserved class of NB-LRR protein. Mol Plant Microbe Interact. 2011;24: 918–931.
49. Zhong Y, Cheng Z-MM. A unique RPW8-encoding class of genes that originated in early land plants and evolved through domain fission, fusion, and duplication. Sci Rep. 2016;6: 32923.
50. Bentham AR, Zdrzalek R, De la Concepcion JC, Banfield MJ. Uncoiling CNLs: Structure/Function Approaches to Understanding CC Domain Function in Plant NLRs. Plant Cell Physiol. 2018;59: 2398–2408.
51. Greenwald J, Buhtz C, Ritter C, Kwiatkowski W, Choe S, Maddelein M-L, et al. The mechanism of prion inhibition by HET-S. Mol Cell. 2010;38: 889–899.
52. Seuring C, Greenwald J, Wasmer C, Wepf R, Saupe SJ, Meier BH, et al. The mechanism of toxicity in HET-S/HET-s prion incompatibility. PLoS Biol. 2012;10: e1001451.
53. Daskalov A, Habenstein B, Sabaté R, Berbon M, Martinez D, Chaignepain S, et al. Identification of a novel cell death-inducing domain reveals that fungal amyloid-controlled programmed cell death is related to necroptosis. Proc Natl Acad Sci U S A. 2016;113: 2720–2725.
54. McDowell JM, Cuzick A, Can C, Beynon J, Dangl JL, Holub EB. Downy mildew (Peronospora parasitica)

resistance genes in Arabidopsis vary in functional requirements for NDR1, EDS1, NPR1 and salicylic acid accumulation. Plant J. 2000;22: 523–529.

55. Tsuchiya T, Eulgem T. An alternative polyadenylation mechanism coopted to the Arabidopsis RPP7 gene through intronic retrotransposon domestication. Proc Natl Acad Sci U S A. 2013;110: E3535–43.
56. Guo YL, Fitz J, Schneeberger K, Ossowski S, Cao J, Weigel D. Genome-wide comparison of nucleotide-binding site-leucine-rich repeat-encoding genes in Arabidopsis. Plant Physiol. 2011;157: 757–769.
57. Rowan BA, Seymour DK, Chae E, Lundberg DS, Weigel D. Methods for Genotyping-by-Sequencing. In: White SJ, Cantsilieris S, editors. Genotyping: Methods and Protocols. New York, NY: Springer New York; 2017. pp. 221–242.
58. Grimm DG, Roqueiro D, Salomé PA, Kleeberger S, Greshake B, Zhu W, et al. easyGWAS: A Cloud-Based Platform for Comparing the Results of Genome-Wide Association Studies. Plant Cell. 2017;29: 5–19.
59. Holub EB, Beynon JL. Symbiology of Mouse-Ear Cress (Arabidopsis Thaliana) and Oomycetes. In: Andrews JH, Tommerup IC, Callow JA, editors. Advances in Botanical Research. Academic Press; 1997. pp. 227–273.
60. Nemri A, Atwell S, Tarone AM, Huang YS, Zhao K, Studholme DJ, et al. Genome-wide survey of Arabidopsis natural variation in downy mildew resistance using combined association and linkage mapping. Proc Natl Acad Sci U S A. 2010;107: 10302–10307.
61. Jorgensen TH, Emerson BC. Functional variation in a disease resistance gene in populations of Arabidopsis thaliana. Mol Ecol. 2008;17: 4912–4923.
62. 1001 Genomes Consortium. Electronic address: magnus.nordborg@gmi.oeaw.ac.at, 1001 Genomes Consortium. 1,135 Genomes Reveal the Global Pattern of Polymorphism in Arabidopsis thaliana. Cell. 2016;166: 481–491.
63. Zimmermann L, Stephens A, Nam S-Z, Rau D, Kübler J, Lozajic M, et al. A Completely Reimplemented MPI Bioinformatics Toolkit with a New HHpred Server at its Core. J Mol Biol. 2018;430: 2237–2243.
64. Maheshwari S, Barbash DA. The genetics of hybrid incompatibilities. Annu Rev Genet. 2011;45: 331–355.
65. Alcázar R, von Reth M, Bautor J, Chae E, Weigel D, Koornneef M, et al. Analysis of a plant complex resistance gene locus underlying immune-related hybrid incompatibility and its occurrence in nature. PLoS Genet. 2014;10: e1004848.
66. Van de Weyer A-L, Monteiro F, Furzer OJ, Nishimura MT, Cevik V, Witek K, et al. The Arabidopsis thaliana pan-NLRome [Internet]. bioRxiv. 2019. p. 537001. doi:10.1101/537001
67. Chae E, Tran DTN, Weigel D. Cooperation and Conflict in the Plant Immune System. PLoS Pathog. 2016;12: e1005452.
68. Yang X, Wang W, Coleman M, Orgil U, Feng J, Ma X, et al. Arabidopsis 14-3-3 lambda is a positive regulator of RPW8-mediated disease resistance. Plant J. 2009;60: 539–550.
69. Jones JDG, Vance RE, Dangl JL. Intracellular innate immune surveillance devices in plants and animals.

Science. 2016;354. doi:10.1126/science.aaf6395

70. Saur IM, Bauer S, Kracher B, Lu X, Franzeskakis L, Müller MC, et al. Multiple pairs of allelic MLA immune receptor-powdery mildew AVRA effectors argue for a direct recognition mechanism. Elife. 2019;8. doi:10.7554/eLife.44471
71. Wang W, Devoto A, Turner JG, Xiao S. Expression of the membrane-associated resistance protein RPW8 enhances basal defense against biotrophic pathogens. Mol Plant Microbe Interact. 2007;20: 966–976.
72. Sáenz-Mata J, Jiménez-Bremont JF. HR4 gene is induced in the Arabidopsis-Trichoderma atroviride beneficial interaction. Int J Mol Sci. 2012;13: 9110–9128.
73. Berkey R, Zhang Y, Ma X, King H, Zhang Q, Wang W, et al. Homologues of the RPW8 Resistance Protein Are Localized to the Extrahaustorial Membrane that Is Likely Synthesized De Novo. Plant Physiol. 2017;173: 600–613.
74. Murphy JM, Czabotar PE, Hildebrand JM, Lucet IS, Zhang J-G, Alvarez-Diaz S, et al. The pseudokinase MLKL mediates necroptosis via a molecular switch mechanism. Immunity. 2013;39: 443–453.
75. Hildebrand JM, Tanzer MC, Lucet IS, Young SN, Spall SK, Sharma P, et al. Activation of the pseudokinase MLKL unleashes the four-helix bundle domain to induce membrane localization and necroptotic cell death. Proc Natl Acad Sci U S A. 2014;111: 15072–15077.
76. Su L, Quade B, Wang H, Sun L, Wang X, Rizo J. A plug release mechanism for membrane permeation by MLKL. Structure. 2014;22: 1489–1500.
77. Wang H, Sun L, Su L, Rizo J, Liu L, Wang L-F, et al. Mixed lineage kinase domain-like protein MLKL causes necrotic membrane disruption upon phosphorylation by RIP3. Mol Cell. 2014;54: 133–146.
78. Chen X, Li W, Ren J, Huang D, He W-T, Song Y, et al. Translocation of mixed lineage kinase domain-like protein to plasma membrane leads to necrotic cell death. Cell Res. 2014;24: 105–121.
79. Wang W, Zhang Y, Wen Y, Berkey R, Ma X, Pan Z, et al. A comprehensive mutational analysis of the Arabidopsis resistance protein RPW8.2 reveals key amino acids for defense activation and protein targeting. Plant Cell. 2013;25: 4242–4261.
80. Glass NL, Kaneko I. Fatal attraction: nonself recognition and heterokaryon incompatibility in filamentous fungi. Eukaryot Cell. 2003;2: 1–8.
81. Daskalov A, Habenstein B, Martinez D, Debets AJM, Sabaté R, Loquet A, et al. Signal transduction by a fungal NOD-like receptor based on propagation of a prion amyloid fold. PLoS Biol. 2015;13: e1002059.
82. Daskalov A, Paoletti M, Ness F, Saupe SJ. Genomic clustering and homology between HET-S and the NWD2 STAND protein in various fungal genomes. PLoS One. 2012;7: e34854.
83. Daskalov A, Dyrka W, Saupe SJ. Theme and variations: evolutionary diversification of the HET-s functional amyloid motif. Sci Rep. 2015;5: 12494.
84. Daskalov A. On the evolutionary trajectories of signal-transducing amyloids in fungi and beyond. Prion. 2016;10: 362–368.

85. Loquet A, Saupe SJ. Diversity of Amyloid Motifs in NLR Signaling in Fungi. Biomolecules. 2017;7. doi:10.3390/biom7020038
86. Cai X, Chen J, Xu H, Liu S, Jiang Q-X, Halfmann R, et al. Prion-like polymerization underlies signal transduction in antiviral immune defense and inflammasome activation. Cell. 2014;156: 1207–1222.
87. Thomma BP, Nürnberger T, Joosten MH. Of PAMPs and effectors: the blurred PTI-ETI dichotomy. Plant Cell. 2011;23: 4–15.
88. Shaner NC, Campbell RE, Steinbach PA, Giepmans BNG, Palmer AE, Tsien RY. Improved monomeric red, orange and yellow fluorescent proteins derived from Discosoma sp. red fluorescent protein. Nat Biotechnol. 2004;22: 1567–1572.
89. Ossowski S, Schneeberger K, Clark RM, Lanz C, Warthmann N, Weigel D. Sequencing of natural strains of Arabidopsis thaliana with short reads. Genome Res. 2008;18: 2024–2033.
90. Li H, Durbin R. Fast and accurate short read alignment with Burrows-Wheeler transform. Bioinformatics. 2009;25: 1754–1760.
91. Cao J, Schneeberger K, Ossowski S, Günther T, Bender S, Fitz J, et al. Whole-genome sequencing of multiple Arabidopsis thaliana populations. Nat Genet. Nature Research; 2011;43: 956–963.
92. Lippert C, Listgarten J, Liu Y, Kadie CM, Davidson RI, Heckerman D. FaST linear mixed models for genome-wide association studies. Nat Methods. 2011;8: 833–835.
93. Schneeberger K, Hagmann J, Ossowski S, Warthmann N, Gesing S, Kohlbacher O, et al. Simultaneous alignment of short reads against multiple genomes. Genome Biol. 2009;10: R98.
94. Edgar RC. MUSCLE: multiple sequence alignment with high accuracy and high throughput. Nucleic Acids Res. 2004;32: 1792–1797.
95. Stamatakis A. RAxML version 8: a tool for phylogenetic analysis and post-analysis of large phylogenies. Bioinformatics. 2014;30: 1312–1313.

Supplemental Information

RPW8/HR Repeats Predict NLR-dependent Hybrid Performance

Cristina A. Barragan, Rui Wu, Sang-Tae Kim, Wanyan Xi, Anette Habring, Jörg Hagmann, Anna-Lena Van de Weyer, Maricris Zaidem, William Wing Ho Ho, George Wang, Ilja Bezrukov, Detlef Weigel, Eunyoung Chae

Supplemental Tables

Table S1. Rescue of hybrid necrosis by amiRNAs against *RPP7* homologs. Related to Figure 1.
Table S2. GWAS hits on chromosome 3 from Lerik1-3 x 80 accessions panel. Related to Figure 2.
Table S3. Rescue effects of amiRNAs targeting *RPW8* homologs. Related to Figure 1 and Figure 3.
Table S4. Accessions for *HR4* survey. Related to Figure 6.
Table S5. Accessions for *RPW8.1* survey. Related to Figure 6.
Table S6. Hybrid necrosis in F_1 plants of Lerik1-3 crossed to other accessions. Related to Figure 6.
Table S7. Hybrid necrosis in F_1 plants of Mrk-0 F_1 crossed to other accessions. Related to Figure 6.
Table S8. Accessions and hybrids in which growth was analyzed with the automated phenotyping platform RAPA. Related to Figure 6.
Table S9. Resistance to the *H. arabidopsidis* isolate Hiks1. Related to Figure S6.
Table S10. Oligonucleotides used for amplifying *RPW8.1/HR4* genomic fragments and swap constructs. Related to Figure 3 and Figure 5.
Table S11. Construct list.

Supplemental Figures

Figure S1. Role of the *RPP7* cluster in *DM6-DM7* dependent hybrid necrosis. Related to Figure 1.
Figure S2. Phenotypic variation in Lerik1-3 F_1 hybrids. Related to Figure 1.
Figure S3. *HR4* and *RPW8.1* CRISPR/Cas9 knockout lines. Related to Figure 3 and Figure S6.
Figure S4. Hybrid necrosis by introduction of natural *HR4* alleles or chimeras.
Related to Figure 3 and Figure 5.
Figure S5. Predicted lengths of *HR4* and *RPW8.1* coding sequences from remapping of short reads from the 1001 Genomes Project. Related to Figure 6.
Figure S6. Resistance and susceptibility to *H. arabidopsidis* isolate Hiks1. Related to Figure S3.

Supplemental Experimental Procedures

Supplemental References

Supplemental Tables

Table S1. Rescue of hybrid necrosis by amiRNAs against *RPP7* homologs. Related to Figure 1.

amiRNA	Sequence	Predicted Col-0 targets	Rescue			
			Mrk-0 x KZ10	Lerik1-3 x Fei-0	Lerik1-3 x ICE106	ICE79 x Don-0
EK19	TAAATGACCATATTCCTGCTC	AT1G58602, AT1G59218, AT1G58807, AT1G58848, AT1G59124	yes	yes	yes	yes
EK20	TTTTCCAGGTATTTCAGTCAA	AT1G58602, AT1G59218, AT1G58848, AT1G58807, AT1G59124	partial	yes	yes	yes
EK21	TCGAGGTATTTCAATCCGCTT	AT1G58602, AT1G59218, AT1G58807, AT1G58848, AT1G59124	yes	yes	yes	yes
EK22	TAAAGTTAGTTCTTGCTCCCA	AT1G58602, AT1G59218, AT1G58807, AT1G58848, AT1G59124	yes	yes	not tested	not tested
EK26	TTAGATCACGTTTTAGCCCAG	AT1G58390	no	no	no	no
EK27	TATGTCTAGATAGATCGGCAA	AT1G58400, 3' portion	no	no	not tested	not tested
EK28	TAAGTTAGTTTTGTGATGCGC	AT1G58400, 5' portion	partial	no	not tested	not tested
EK29	TCTTAATTCATGCATCCGCAT	AT1G58390, 3' portion	no	no	no	no
EK30	TATATCAGACGCAAGTTCCCT	AT1G58410	no	no	not tested	not tested
EK31	TAAAGTCGCTTTCGTAGCCGC	AT1G58390, 5' portion	no	no	not tested	not tested

AmiRNAs were designed based on NLR sequences of the *RPP7* cluster in Col-0 (Table S1) using WMD3 (http://wmd3.weigelworld.org/). Constructs were introduced into Mrk-0, Lerik1-3 or ICE79, and T_1 lines were crossed to incompatible parents. Hybrid necrosis was scored at 16°C. Examples of F_1 plants are shown in Figure S1.

Table S2. GWAS hits on chromosome 3 from Lerik1-3 x 80 accessions panel and tagging SNPs present in accessions carrying different HR4 types. Related to Figure 2.

		HR4 type			
		1	2	5	6
Position	-log(P-value)	No-0	ICE21	ICE106	TueWa1-2
18,743,818	26.95	A	A	***G***	***G***
18,745,470	11.22	C	***T***	***T***	***T***
18,741,733	8.67	C	C	C	C
18,742,020	8.67	G	G	G	G
18,742,285	8.67	G	G	G	G
18,742,408	8.67	C	C	C	C
18,742,741	8.67	G	G	G	G
18,742,864	8.67	T	T	T	T
18,741,725	8.08	A	A	A	A
18,742,108	8.08	A	*NA*	A	A
18,742,821	8.08	C	C	C	C

Location of *HR4* (At3g50480) is 18,733,287 to 18,734,180 bp on chromosome 3 of the reference Col-0 genome. The next protein-coding gene is At3g50500 (18,741,805 to 18,743,904 bp), with At3g50490 (18,738,630 to 18,739,261 bp) encoding a transposable element (see Figure 4a). SNPs in bold italics differ from the Col-0 reference.

Table S3. Rescue effects of amiRNAs targeting *RPW8* homologs. Related to Figure 1 and Figure 3.

amiRNA	Sequence	Predicted targets	Predicted non-targets	Rescue	
				Lerik1-3 x Fei-0	Lerik1-3 x ICE106
MZ110	TTCAAGGAAACACGTGAGACG	*RPW8.1a*, *RPW8.1b*, *HR4*	*RPW8.2*	partial	partial
MZ137	TGATACTAATGATTGTAGCGC	*RPW8.1b*	*RPW8.1a*, *HR4*	no	not tested
MZ141	TCAGAACGTAAATCGGATCGC	*RPW8.2* homolog	*RPW8.1*, *HR4*	no	not tested
KB amiR-RPW8.1 b	TATGATTGTAGCGCAGAGACG	*RPW8.1a*, *RPW8.1b*	*HR4*	no	not tested
ACBHR4.2	TCTTAATTCATGCATCCGCAT	*HR4*	*RPW8.1a*, *RPW8.1b*	yes	yes

AmiRNAs were designed based on sequence information of *RPW8*/*HR* clusters from Col-0, Ms-0 and KZ10. Constructs were introduced into Fei-0 or ICE106, and T_1 lines were crossed to the incompatible accession Lerik1-3. Hybrid necrosis was scored at 16°C. Parental genotypes and the presence of amiRNA constructs were confirmed with by PCR genotyping (see Figure 3a).

Table S4. Accessions for *HR4* survey. Related to Figure 6.

Accession	1001 Genomes Project ID	Stock center ID	*HR4* type	*HR4* haplotype	Covered region (bp)
IP-Tol-7	9588	CS77371	1	XV	885
IP-Trs-0	9590	CS77387	1	XV	880
El-0	7117	CS76479	1	XIV	894
Wu-0	7415	CS78858	1	XIV	835
Castelfed-1-199	9683	CS76748	1	XIII	887
ICE79/Voeran-1	9979	CS76352	1	XIII	868
T960	6148	CS77325	1	XII	894
ICE60/Stepn-2	9955	CS76377	1	XI	773
ICE36/Dobra-1	10018	CS76369	1	X	848
No-0	7273	CS77128	1	X	802
Knjas-1	9749	CS76971	1	X	834
LP3413.31	8464	CS79030	1	IX	894
Zdarec3	403	CS78873	1	IX	894
Del-10	10016	CS76397	1	IX	554
Lan-0	7208	CS76539	1	IX	894
Col-0	6909	CS76539	1	IX	894
Noveg-3	9638	CS77133	1	IX	894
Pu2-7	6956	CS76580	1	IX	894
Wil-2	7413	CS78856	1	IX	894
PT2.21	8077	CS77191	1	IX	894
Bsch-0	7031	CS76457	1	IX	890
Wc-1	7404	CS76627	2	V	887
Ven-1	7384	CS76624	2	V	856
UKNW06-481	5644	CS78798	2	V	885
Tu-0	7375	CS76617	2	V	894
ICE21/Petro-1	10017	CS76370	2	V	778
Lu-1	8334	CS77056	2	V	863
LIN-S-5	915	CS77040	2	V	785
Tsu-0	7373	CS77389	2	V	847
Bd-0	7013	CS76445	2	V	854
Bai-10	9779	CS76682	2	V	871
Kus3-1	9802	CS76991	2	V	877
Lag1-4	9102	CS76999	2	IV	894
Lag1-5	9103	CS77000	2	IV	894
HKT2-4	9995	CS76404	2	V	789
Dr-0	7106	CS78897	2	V	875
Pi-0	7298	CS76572	2	V	880
For-2	5741	CS78783	2	V	844
Erg2-6	9784	CS76845	2	V	892
Bay-0	6899	CS22633	2	V	-
Sq-8	6967	CS76604	2	V	889

Li-7	7231	CS77035	2	VI	879
Bs-1	7003	CS78888	2	V	894
Tottarp-2	6243	CS77381	2	V	838
Xan-6	9070	CS78862	2	VII	883
Nemrut-1	9993	CS76398	2	VII	837
Lerik2-3	9081	CS77026	2	VII	878
Xan-5	9069	CS78861	2	VII	890
Ty-1	7351	CS78790	3	III	854
Or-1	6074	CS77150	3	III	834
Bil-5	6900	CS76709	3	III	805
T510	6109	CS77301	3	III	892
Mnz-0	7244	CS76552	3	III	884
Bil-7	6901	CS76710	3	III	859
Cimin-1	9661	CS76771	4	VIII	865
ICE112/Moran-1	9967	CS76427	4	VIII	850
Bivio-1	9649	CS76713	5	II	618
Cdm-0	9943	CS76410	5	II	668
IP-Mot-0	9560	CS77109	5	II	558
Nicas-1	9658	CS77127	5	II	46
Wei-0	6979	CS76628	5	II	641
Rhen-1	7316	CS78916	5	II	555
ICE106/Mammo-1	9964	CS76365	5	II	557
ICE92/Angit-1	9981	CS76366	5	II	510
IP-Bea-0	9522	CS76695	5	II	618
IP-Ala-0	9515	CS76650	5	II	558
IP-Cum-1	9537	CS76787	5	II	610
Paw-26	2171	CS77164	5	II	497
IP-Vav-0	9511	CS78835	5	II	581
KBG2-13	9770	CS76966	5	II	653
ICE107/Mammo-2	9965	CS76364	5	II	668
Com-1	7092	CS76469	5	II	638
UKID74	5779	CS78789	5	II	615
PHW-34	8244	CS77174	5	II	592
PLO-1	9923	CS77180	5	II	867
IP-Tri-0	9900	CS77386	5	II	650
ICE7/Lecho-1	9987	CS76371	5	II	626
RUM-20	9925	CS77226	5	II	483
Lu4-2	9792	CS77058	5	II	652
Gy-0	8214	CS78901	5	II	655
Ra-0	6958	CS76582	5	II	566
IP-Fue-2	9541	CS76871	5	II	880
Nie1-2	9996	CS76402	5	II	466
Pra-6	9948	CS76416	5	II	664
328ME059	8584	CS76641	6	I	644
Abd-0	6986	CS76429	6	I	433

CIBC-5	6908	CS78894	6	I	367
Cnt-1	5726	CS78782	6	I	294
Durh-1	7107	CS76477	6	I	243
Edinburgh-1	9298	CS76832	6	I	341
Fei-0	9941	CS76412	6	I	346
Ha-0	7163	CS76500	6	I	356
Hart-2	9799	CS76913	6	I	377
HR-10	6923	CS76940	6	I	317
IP-Rds-0	9573	CS77206	6	I	361
Kin-0	6926	CS76527	6	I	325
Liri-1	9654	CS77041	6	I	65
Mdn-1	1829	CS77077	6	I	314
NFA-8	6944	CS78913	6	I	367
PNA3.40	7947	CS77184	6	I	303
Pog-0	7306	CS76576	6	I	294
QUI-8	9934	CS77199	6	I	894
Rmx-A180	7525	CS77218	6	I	344
Rou-0	7320	CS76591	6	I	243
Sarno-0	9660	CS77236	6	I	330
Seattle-0	7332	CS76598	6	I	324
Ste-40	2317	CS77278	6	I	284
TueScha-9	10000	CS76401	6	I	413
TueWa1-2	10002	CS76405	6	I	414
UKNW06-003	5353	CS78792	6	I	343
UKNW06-403	5577	CS78797	6	I	296
UKSE06-533	5276	CS78806	6	I	307
Uod-1	6975	CS76621	6	I	314
Vind-1	7387	CS76625	6	I	252

Covered region indicates the length of *HR4*$^{Col-0}$ (894 bp) covered by reads from the 1001 Genomes Project (http://1001genomes.org), allowing for five mismatches. *HR4* types are categorized according to the number of *RPW8*/*HR* repeats, and the haplotype is based on the entire *HR4* coding sequence.

Table S5. Accessions for *RPW8.1* survey. Related to Figure 6.

Accession	1001 Genomes Project ID	Stock center ID	*RPW8.1* type	Covered region (bp)
KZ-10	10019	CS28435	1	749
KZ-9	6931	CS76537	1	749
Lebja-2	9632	CS77016	1	749
Shu-1	14318	CS78930	1	749
Ulies-1	9737	CS78815	1	749
Lebja-1	9631	CS77015	1	749
Kolyv-3	9626	CS76978	1	749
Knox-10	6927	CS76973	2	741
Ang-0	6992	CS76436	2	735
Kolyv-6	9628	CS76980	2	727
Lag2-2	9990	CS76390	2	713
IP-Pro-0	9571	CS78914	2	713
Qui-0	9949	CS76417	2	708
Uk-1	7378	CS76620	2	697
Ms-0	6938	CS76555	3	672
Tamm-2	6968	CS76610	3	657
TueWa1-2	10002	CS76405	3	568
TueScha-9	10000	CS76401	3	501
Fei-0	9941	CS76412	3	461
En-1	8290	CS76841	3	414
Hn-0	7165	CS76513	3	315
CIBC-5	6908	CS78894	3	301
NFA-8	6944	CS78913	3	295
Ha-0	7163	CS76500	3	197
Bg-2	6709	CS28069	3	186
Yeg-4	9130	CS78865	3	130
Yeg-5	9131	CS78866	3	0
Yeg-2	9128	CS78864	3	0

Table S6. Hybrid necrosis in F_1 plants of Lerik1-3 crossed to other accessions. Related to Figure 6.

Cross	*HR4* type	Hybrid necrosis
Lerik1-3 x Col-0	1	none
Lerik1-3 x Noveg-3	1	none
Lerik1-3 x Lerik2-3	2	none
Lerik1-3 x Ven-1	2	none
Ty-1 x Lerik1-3	3	none
Lerik1-3 x Bil-5	3	none
Lerik1-3 x Bil-7	3	none
Lerik1-3 x Or-1	3	none
Lerik1-3 x ICE112	4	none
Lerik1-3 x Cimin-1	4	none
Lu4-2 x Lerik1-3	5	mild
Lerik1-3 x Lu4-2	5	mild
Lerik1-3 x Tri-0	5	mild
Nicas-1 x Lerik1-3	5	mild
Lerik1-3 x IP-Cum	5	mild
Lerik1-3 x RUM20	5	mild
Lerik1-3 x PAW26	5	mild
Uod-1 x Lerik1-3	6	intermediate
Lerik1-3 x Liri-1	6	intermediate
Lerik1-3 x Vind-1	6	strong
Ste40 x Lerik1-3	6	strong
Pog-0 x Lerik1-3	6	strong
Lerik1-3 x RmxA180	6	strong
Lerik1-3 x Edinburgh-1	6	strong
Lerik1-3 x PNA3.40	6	strong

Strong hybrid necrosis equals what is observed in Lerik1-3 x Fei-0 F_1 hybrids.

Table S7. Hybrid necrosis in F_1 plants of Mrk-0 F_1 crossed to other accessions. Related to Figure 6.

Cross	*RPW8.1* type	Hybrid necrosis
Mrk-0 x KZ-10	1	strong
Mrk-0 x KZ-9	1	strong
Mrk-0 x Lebja-2	1	strong
Mrk-0 x Shu-1	1	mild
Mrk-0 x Ulies-1	1	strong
Mrk-0 x Lebja-1	1	mild
Mrk-0 x Kolyv-3	1	strong
Mrk-0 x Knox-10	2	none
Mrk-0 x Ang-0	2	none
Mrk-0 x Kolyv-6	2	none
Mrk-0 x Lag2-2	2	none
Mrk-0 x IP-Pro-0	2	none
Mrk-0 x Qui-0	2	none
Mrk-0 x Uk-1	2	none
Mrk-0 x Ms-0	3	none
Mrk-0 x Tamm-2	3	none
TueWa1-2 x Mrk-0	3	none
TueScha-9 x Mrk-0	3	none
Fei-0 x Mrk-0	3	none
Mrk-0 x En-1	3	none
Mrk-0 x Hn-0	3	none
Mrk-0 x Wei-0	3	none
Mrk-0 x CIBC-5	3	none
Mrk-0 x NFA-8	3	none
Mrk-0 x Ra-0	3	none
Mrk-0 x Ha-0	3	none
Mrk-0 x Bg-2	3	none
Yeg-4 x Mrk-0	3	none
Mrk-0 x Yeg-5	3	none
Mrk-0 x Yeg-2	3	none

Strong hybrid necrosis equals what is observed in KZ10 x Mrk-0 hybrids.

Table S8. Accessions and hybrids in which growth was analyzed with the automated phenotyping platform RAPA. Related to Figure 6.

Population	*HR4* type
Lerik1-3	-
Lerik1-3 x TueWa1-2	6
TueWa1-2	
TueScha-9 x Lerik1-3	
TueScha-9	
Lerik1-3 x Fei-0	
Fei-0	
Lerik1-3 x ICE106	5
ICE106	
Nie1-2 x Lerik1-3	
Nie1-2	
Lerik1-3 x Cdm-0	
Cdm-0	
Lerik1-3 x HKT2-4	2
HKT2-4	
Lerik1-3 x ICE21	
ICE21	
Nemrut-1 x Lerik1-3	
Nemrut-1	
ICE36 x Lerik1-3	1
ICE36	
ICE60 x Lerik1-3	
ICE60	
ICE79 x Lerik1-3	
ICE79	

Table S9. Resistance to the *H. arabidopsidis* isolate Hiks1. Related to Figure S6.

	Accession / F_1 cross	**Hiks1 resistance***
Accessions	Col-0	weak resistance
	Lerik1-3	strong resistance
	ICE106	no resistance
	Fei-0	no resistance
Positive infection controls	Col-0 *eds1-1*	no resistance
	Ws-0	no resistance
	Ws-0 *eds1-1*	no resistance
	Oy-0	no resistance
	Col-0 *rpp7-15*	no resistance
Col-0 *HR4 CRISPR/Cas9 KOs*	Col-0 *hr4* #6/8	strong resistance
	Col-0 *hr4* #8/18	strong resistance
Lerik1-3 amiR-RPP7 transgenics†	EK29b	strong resistance
	EK28a	strong resistance
	EK27	strong resistance
	EK26	strong resistance
	EK22	strong resistance
	EK21	strong resistance
	EK19	strong resistance
F_1 hybrids	Lerik1-3 x Fei-0	strong resistance
	Lerik1-3 x ICE106	weak resistance

*strong resistance: no conidiophores; weak resistance: 1-5 conidiophores/cotyledon, with some sporulation; very weak resistance: 6-19 conidiophores/cotyledon, with low to medium sporulation; no resistance: >20 conidiophores/cotyledon, heavy sporulation.

†See Table S1 for amiRNA key.

Table S10. Oligonucleotides used for amplifying *RPW8.1/HR4* genomic fragments and swap constructs. Related to Figure 3 and Figure 5.

Primer	Sequence	Purpose
G-41108	GCCACATTGGTCTCTCAATTTGT	PCR *HR4* genomic fragments
G-40245	CTCCATTAATCTGCAAATTTGCTAA	
G-40185	TCTGGGCTAATTCAAATTTCATAT	
G-12714	GACCCGTACAGTACTAAGTCTA	
G-41573	CAATCATTGTTGGGAAGAAGAAAGA	
G-41558	gctcttcaATGCCGATTGGTGAGCTTGC	PCR *RPW8.1* genomic fragments
G-39847	TAGATCATTGTCAGTAAA	
G-37615	AGATAAGCCATAGAACCTCAGTGATAC	Lerik1-3 ClaI CAPS
G-37616	GGTTTGCTGCTTCCTTCTAAATACATT	
G-37354	TAAGTCTTGCATATCAGGCATTTCATC	ICE79 ClaI CAPS
G-37355	TATTTGTAGCTTTAGAAGTTGAGGCTG	
G-36173	CCAATGAACTCTATTTCAGGAATCTGG	Don-0 XhoI CAPS
G-36174	AGAGCGGGAAGAAATATCAGATTAAGA	
G-37109	CTGATGATACTTTGTGATTCCAGGATG	Fei-0 XhoI CAPS
G-37110	AGTTCAATTTCACAGGTCTACCATAGA	
G-36261	ATCAAAGTAAATCACAGGAGCATCATC	ICE106 XbaI CAPS
G-36262	GAGAGCTTTGAAACTGAACAAGAAGTA	
G-41539	gctcttcaagtTGTCCCAATTGTGTCAAACGACTC	*RPW8.1*^{KZ10} promoter
G-41556	gctcttcacatTTTTTTAAAGTAGTTGTTTAGCTCTCGAGG	
G-41558	see above	*RPW8.1*$^{Ms-0}$ CDS truncation
G-41925	gctcttctATCAACTTGAAAATCCACAACTATTATGC	
G-41558	see above	*RPW8.1*^{KZ10} CDS truncation
G-41924	gctcttctATCAACTTGAAAATCCACAACTATTATCC	
G-41558	see above	*RPW8.1*$^{Ms-0}$ CDS truncation +TAG
G-42151	gctcttcaccaCTAATCAACTTGAAAATCCACAACTATTAT	
G-41558	see above	*RPW8.1*^{KZ10} CDS truncation +TAG
G-42150	gctcttcaccaCTAATCAACTTGAAAATCCACAACTATTATCC	
G-41927	gctcttcaagtGCCACATTGGTCTCTCAATTTGT	*HR4*$^{Fei-0}$ promoter
G-41928	gctcttcacatTTTTTTTAAGTAGTTCTTTAGCTCTCGA	
G-41929	gctcttcaATGCCGCTTCTTGAGCTTGC	*HR4*$^{Fei-0}$ CDS truncation
G-41930	gctcttcaCTCAAGTACTAGCCTTACTAATTCAAGTT	
G-41929	see above	*HR4*^{ICE106} CDS truncation
G-41931	gctcttcaCTCAAGTACTACCCTTACTAATTCAAGTT	
G-41932	gctcttcaATGCCGATTGCTGAGCTTGC	*HR4*$^{Col-0}$ CDS truncation
G-41933	gctcttcaCTCACGTGCTACCCTTACTAATTCAAGTT	
G-41929	see above	*HR4*$^{Fei-0}$ CDS truncation + TAG
G-42152	gctcttcaCCACTACTCAAGTACTAGCCTTACTAATTCAAGTT	
G-41929	see above	*HR4*^{ICE106} CDS truncation + TAG
G-42153	gctcttcaCCACTACTCAAGTACTACCCTTACTAATTCAAGTT	
G-41932	gctcttcaATGCCGATTGCTGAGCTTGC	*HR4*$^{Col-0}$ CDS truncation + TAG
G-42154	gctcttcaCCACTACTCACGTGCTACCCTTACTAATTCAAGTT	

Table S11. Constructs.

Construct	Description	Backbone	Promoter	CDS
ACB066	genomic *HR4*	pMLBart	*HR4*$^{Fei-0}$	*HR4*$^{Fei-0}$
ACB067	genomic *HR4*	pMLBart	*HR4*^{ICE106}	*HR4*^{ICE106}
ACB011	genomic *RPW8.1a*	pMLBart	*RPW8.1a*$^{Fei-0}$	*RPW8.1a*$^{Fei-0}$
ACB012	genomic *RPW8.1b*	pMLBart	*RPW8.1b*$^{Fei-0}$	*RPW8.1b*$^{Fei-0}$
ACB068	amiR-*RPW8.1*	pFK210	CaMV 35S	see Table S3
MZ110	amiR-*RPW8.1*	pFK210	CaMV 35S	see Table S3
MZ137	amiR-*RPW8.1*	pFK210	CaMV 35S	see Table S3
MZ141	amiR-*RPW8.1*	pFK210	CaMV 35S	see Table S3
KB amiR-RPW8.1 b	amiR-*RPW8.1*	pFK210	CaMV 35S	see Table S3
ACB074	amiR-*RPP7* EK19	pFK210	CaMV 35S	see Table S1
ACB075	amiR-*RPP7* EK20	pFK210	CaMV 35S	see Table S1
ACB076	amiR-*RPP7* EK21	pFK210	CaMV 35S	see Table S1
ACB077	amiR-*RPP7* EK22	pFK210	CaMV 35S	see Table S1
ACB078	amiR-*RPP7* EK26	pFK210	CaMV 35S	see Table S1
ACB079	amiR-*RPP7* EK27	pFK210	CaMV 35S	see Table S1
ACB080	amiR-*RPP7* EK28	pFK210	CaMV 35S	see Table S1
ACB081	amiR-*RPP7* EK29	pFK210	CaMV 35S	see Table S1
ACB082	amiR-*RPP7* EK30	pFK210	CaMV 35S	see Table S1
ACB083	amiR-*RPP7* EK31	pFK210	CaMV 35S	see Table S1
ACB042	*HR4* CRISPR/Cas9 Col-0	pRW006	CaMV 35S	see Figure S3
pWX031	*RPW8.1* CRISPR/Cas9 KZ10	pGGZ001	MAS	see Figure S3
pRW016	*K*-0	pMCY2	*RPW8.1*^{KZ10}	*RPW8.1*^{KZ10}
pRW017	*M*-0	pMCY2	*RPW8.1*^{KZ10}	*RPW8.1*$^{Ms-0}$
pRW020	*M*-Aα	pMCY2	*RPW8.1*^{KZ10}	*RPW8.1*$^{Ms-0}$
pRW021	*K*-Aα	pMCY2	*RPW8.1*^{KZ10}	*RPW8.1*^{KZ10}
pRW018	*K*-Bβ	pMCY2	*RPW8.1*^{KZ10}	*RPW8.1*^{KZ10}
pRW019	*K*-Bcβ	pMCY2	*RPW8.1*^{KZ10}	*RPW8.1*^{KZ10}
ACB085	*K*-BBβ	pMCY2	*RPW8.1*^{KZ10}	*RPW8.1*^{KZ10}
ACB086	*K*-BBcβ	pMCY2	*RPW8.1*^{KZ10}	*RPW8.1*^{KZ10}
ACB087	*M*-BBcβ	pMCY2	*RPW8.1*^{KZ10}	*RPW8.1*$^{Ms-0}$
ACB088	*K*-BBBβ	pMCY2	*RPW8.1*^{KZ10}	*RPW8.1*^{KZ10}
ACB089	*K*-BBBcβ	pMCY2	*RPW8.1*^{KZ10}	*RPW8.1*^{KZ10}
ACB045	*C*-O	pMCY2	*HR4*$^{Fei-0}$	*HR4*$^{Col-0}$
ACB044	*I*-0	pMCY2	*HR4*$^{Fei-0}$	*HR4*^{ICE106}
ACB050	*F*-0	pMCY2	*HR4*$^{Fei-0}$	*HR4*$^{Fei-0}$
ACB046	*C*-QQRSRγ	pMCY2	*HR4*$^{Fei-0}$	*HR4*$^{Col-0}$
ACB048	*F*-QQRSRγ	pMCY2	*HR4*$^{Fei-0}$	*HR4*$^{Fei-0}$
ACB058	*F*-QQSRγ	pMCY2	*HR4*$^{Fei-0}$	*HR4*$^{Fei-0}$
ACB069	*F*-QQRSRδ	pMCY2	*HR4*$^{Fei-0}$	*HR4*$^{Fei-0}$
ACB070	*F*-QQRSδ	pMCY2	*HR4*$^{Fei-0}$	*HR4*$^{Fei-0}$
ACB051	*I*-RT	pMCY2	*HR4*$^{Fei-0}$	*HR4*^{ICE106}

ACB054	*F*-RTδ	pMCY2	*HR4*$^{Fei-0}$	*HR4*$^{Fei-0}$
ACB047	*F*-RRTδ	pMCY2	*HR4*$^{Fei-0}$	*HR4*$^{Fei-0}$
ACB071	*F*-RRTγ	pMCY2	*HR4*$^{Fei-0}$	*HR4*$^{Fei-0}$
ACB053	*C*-Tδ	pMCY2	*HR4*$^{Fei-0}$	*HR4*$^{Col-0}$
ACB052	*I*-Tδ	pMCY2	*HR4*$^{Fei-0}$	*HR4*^{ICE106}
ACB065	*F*-Tδ	pMCY2	*HR4*$^{Fei-0}$	*HR4*$^{Fei-0}$

Supplemental Figures

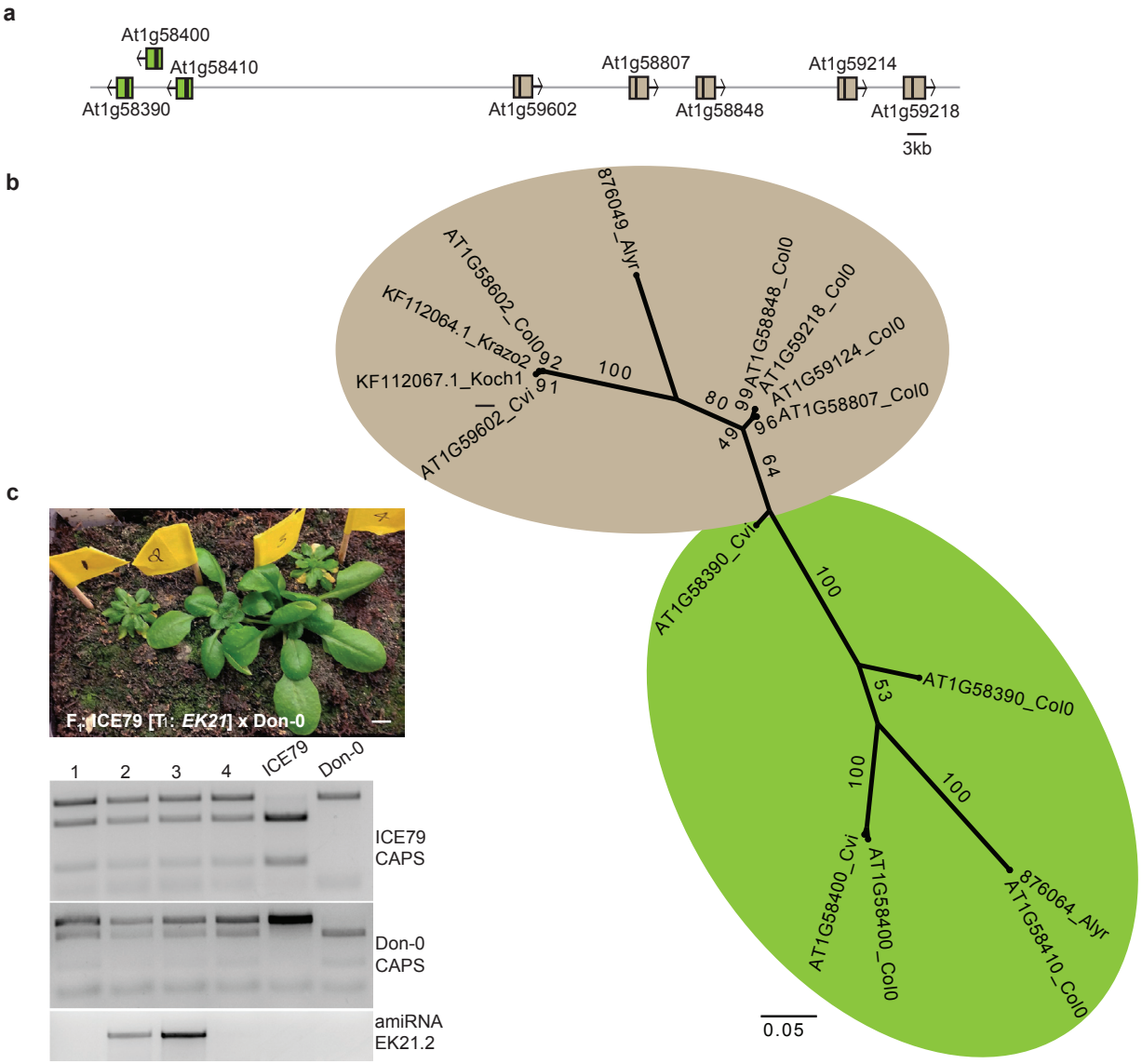

Figure S1. Role of the *RPP7* cluster in *DM6-DM7* dependent hybrid necrosis. Related to Figure 1. **(a)** *RPP7* cluster in the Col-0 reference genome. The left portion of the cluster consists of three *NLR* genes, At1g58390, At1g58400 and At1g58410 (green arrows). The right portion includes five *NLR* genes, At1g58602, At1g58807, At1g58848, At1g59214 and At1g59218 (brown arrows). Twenty-two non-NLR genes in this region are not shown. **(b)** Maximum-likelihood tree of *NLR* genes in the *RPP7* cluster based on the NB domain. At1g59124 and At1g58807 sequences are identical, as are At1g59218 and At1g58848. Same colors as in (A). Bootstrap values (out of 100) are indicated on each branch. **(c)** Representative rescue experiment using an amiRNA construct targeting *RPP7* homologs (see Table S1). ICE79 was transformed with the amiRNA construct EK21 and T_1 plants were crossed to Don-0, resulting in rescued and non-rescued plants segregating in the F_1 progeny. Parental genotypes were confirmed with CAPS markers, shown below. Five-week old plants grown in 16°C are shown.

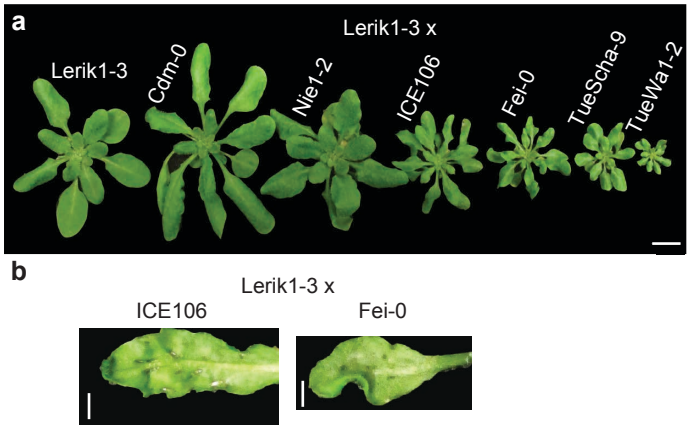

Figure S2. Phenotypic variation in Lerik1-3 F_1 hybrids. Related to Figure 1.
Major differences were observed in rosette size of F_1 hybrids **(a)** and spotted cell death on the abaxial side of leaves **(b)**. Scale bar represents 1cm (a) and 1mm (c). Plants were five weeks old.

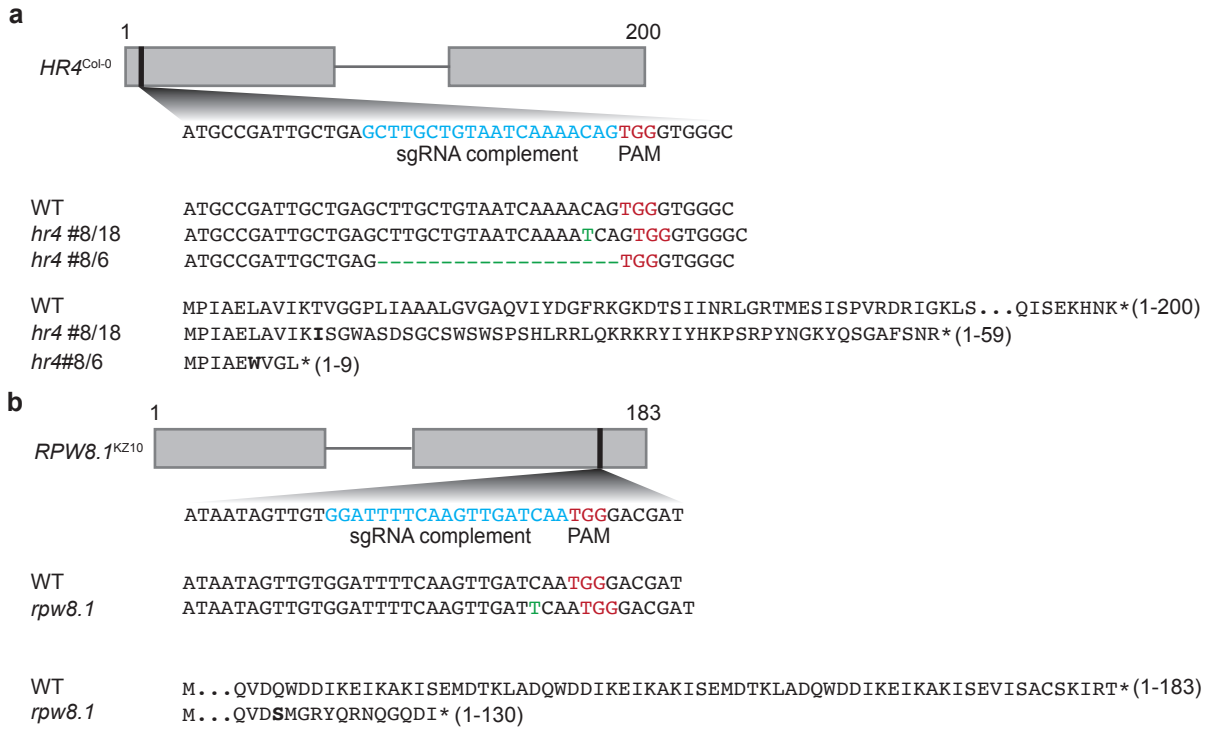

Figure S3. *HR4* and *RPW8.1* CRISPR/Cas9 knockout lines. Related to Figure 3 and Figure S6.
(a) Two alleles of *HR4* in Col-0 with a 1- bp insertion (#8/18) or a 19-bp deletion (#8/6) were identified by amplicon sequencing. **(b)** An allele of *RPW8.1* in KZ10 with a 1-bp insertion was recovered. The stop codons are marked with an asterisk and the first amino acid after a frameshifting event is in bold.

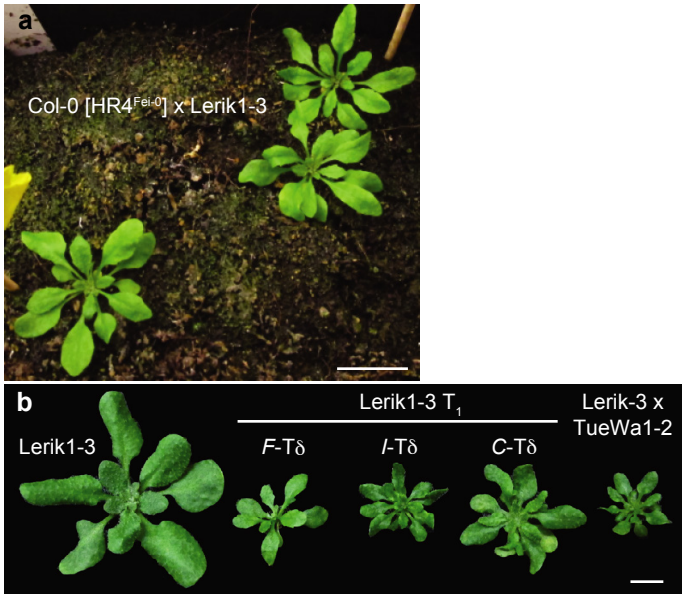

Figure S4. Hybrid necrosis by introduction of natural *HR4* alleles or chimeras. Related to Figure 3 and Figure 5. **(a)** F_1 hybrids from a cross of Lerik1-3 to a Col-0 T_1 plant expressing the *HR4*$^{Fei-0}$ allele. **(b)** Effects of chimeric *HR4* transgenes introduced into Lerik1-3, with negative and positive controls shown to the left and right. Scale bar represents 1cm. Five week-old plants are shown.

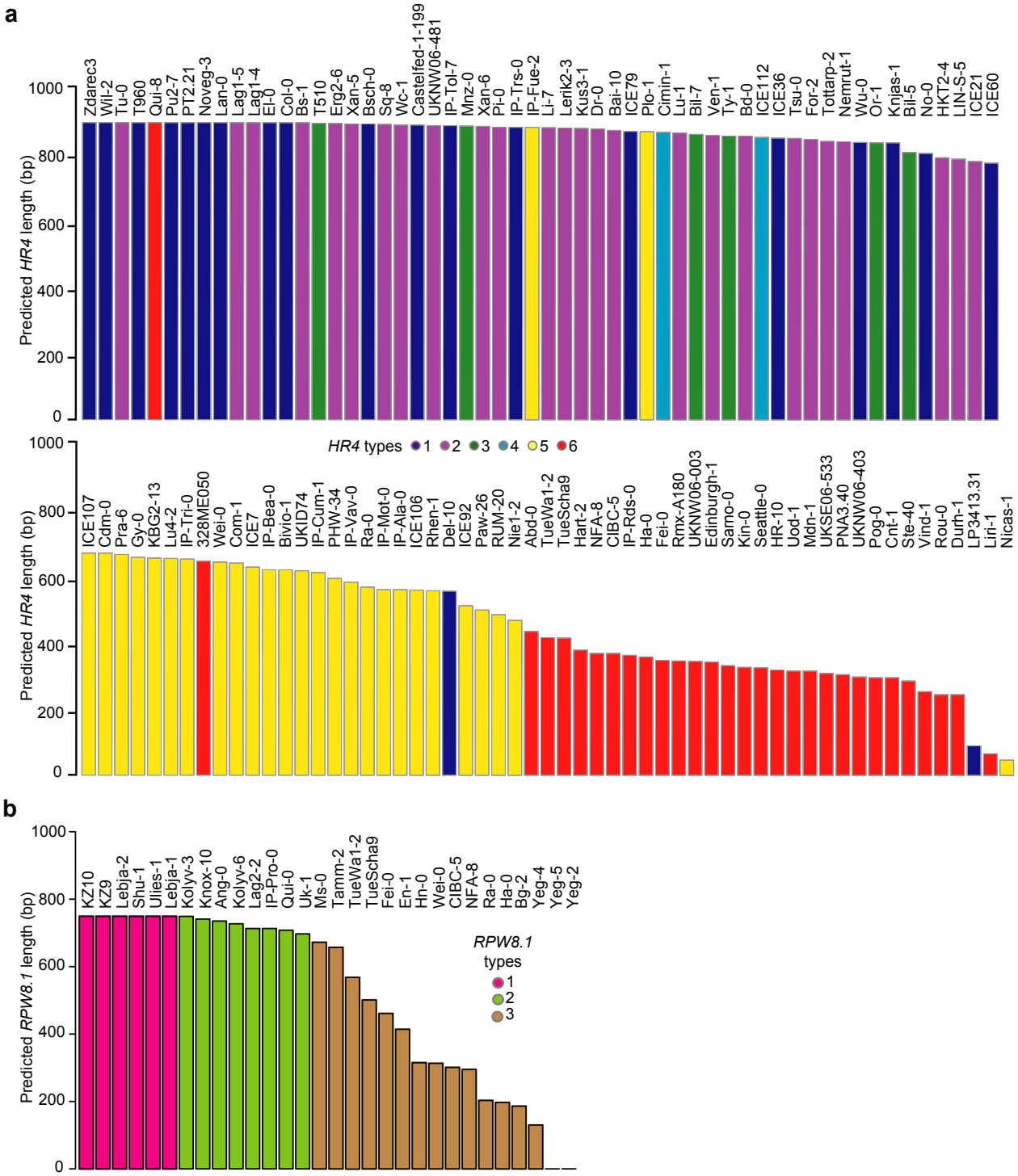

Figure S5. Predicted lengths of *HR4* and *RPW8.1* coding sequences from remapping of short reads from the 1001 Genomes Project. Related to Figure 6.

(a) *HR4* type assignments based on information from Sanger sequencing. **(b)** *RPW8.1* type based on information from Sanger sequencing.

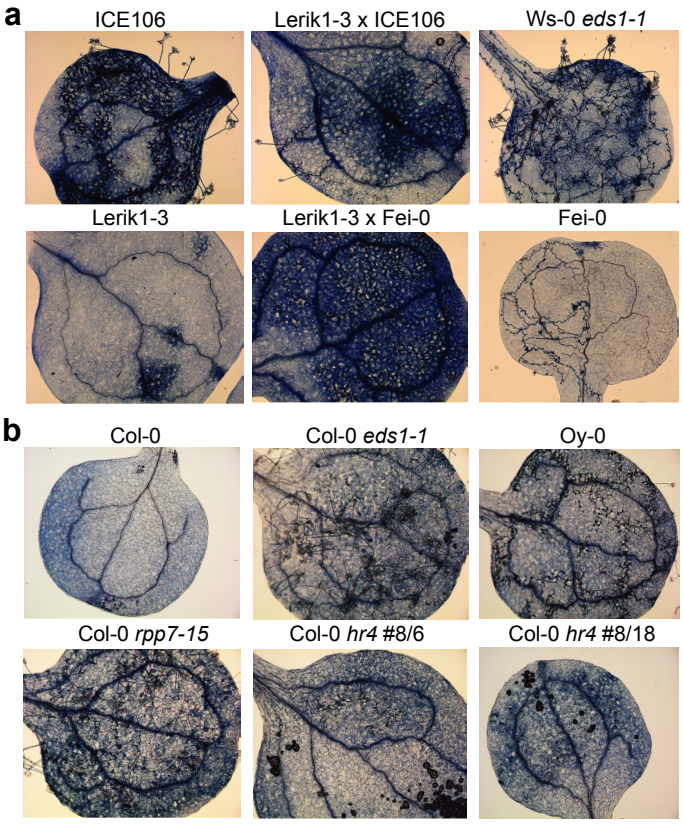

Figure S6. Resistance and susceptibility to *H. arabidopsidis* isolate Hiks1. Related to Figure S3.
(a) Trypan Blue stained cotyledons 5 days after infection. Lerik1-3 is resistant, while Fei-0 and ICE106 are fully susceptible. The F_1 hybrids Lerik1-3 x Fei-0 and Lerik1-3 x ICE106 appear to be less resistant than Lerik1-3. Ws-0 *eds1-1* is a positive infection control. **(b)** Two different *hr4* loss-of-function alleles (see Figure S3) are as resistant as Col-0 wild-type plants. *eds1-1* and *rpp7-15* are positive infection controls.

Supplemental Experimental Procedures

RPP7 phylogeny

The NB domain was predicted using SMART (http://smart.embl-heidelberg.de/). NB amino acid sequences were aligned using MUSCLE [1]. A maximum-likelihood tree was generated using the BLOSUM62 model in RaxML [2]. Topological robustness was assessed by bootstrapping 1,000 replicates.

RAPA phenotyping

Images were acquired daily in top view using two cameras per tray. Cameras were equipped with OmniVision OV5647 sensors with a resolution of 5 megapixels. Each camera was attached to a Raspberry Pi computer (Revision 1.2, Raspberry Pi Foundation, UK) [3]. Images of individual plants were extracted using a predefined mask for each plant. Segmentation of plant leaves and background was then performed by removing the background voxels then a GrabCut-based automatic postprocessing was applied [4]. Lastly, unsatisfactory segmentations were manually corrected. The leaf area of each plant was then calculated based on the segmented plant images.

Pathology

The *Hyaloperonospora arabidopsidis* isolate Hiks1 was maintained by weekly subculturing on susceptible Ws-0 *eds1-1* plants [5]. To assay resistance of susceptibility, 12- to 13-day old seedlings were inoculated with 5×10^4 spores/ml. Sporangiophores were counted 5 days after infection.

Constructs and Transgenic lines

Genomic fragments were PCR amplified, cloned into pGEM®-T Easy (Promega, Madison, WI, USA), and either directly transferred to binary vector pMLBart or Gateway vectors pJLBlue and pFK210. amiRNAs [6] against members of the *RPP7* and *RPW8/HR* clusters were designed using the WMD3 online tool (http://wmd3.weigelworld.org/), and placed under the CaMV 35S promoter in the binary vector pFK210 derived from pGreen [7]. amiRNA constructs were introduced into plants using *Agrobacterium*-mediated transformation [8]. T_1 transformants were selected on BASTA, and crossed to incompatible accessions. For the chimeras, promoters and 5' coding sequences were PCR amplified from genomic DNA , repeat and tail sequences were synthesized using Invitrogen's GeneArt gene synthesis service, all were cloned into pBlueScript. The three parts, promoter, 5' and 3' coding sequences, were assembled using Greengate cloning [9] in the backbone vector pMCY2 [10]. Quality control was done by Sanger sequencing. Transgenic T_1 plants were selected based on mCherry seed fluorescence. For CRISPR/Cas9 constructs, sgRNAs targeting *HR4* or *RPW8.1* were designed on the Chopchop website (http://chopchop.cbu.uib.no/), and assembled using a Greengate reaction into supervector pRW006 (pEF005-sgRNA-shuffle-in [11] Addgene plasmid #104441). mCherry positive T_2 transformants were

screened for CRISPR/Cas9-induced mutations by Illumina MiSeq based sequencing of barcoded 250-bp amplicons. Non-transgenic homozygous T_3 lines were selected based on absence of fluorescence in seed coats.

Supplemental References

1. Edgar, R.C., *MUSCLE: multiple sequence alignment with high accuracy and high throughput.* Nucleic acids research, 2004. **32**(5): p. 1792-1797.
2. Stamatakis, A., *RAxML version 8: a tool for phylogenetic analysis and post-analysis of large phylogenies.* Bioinformatics, 2014. **30**(9): p. 1312-1313.
3. Vasseur, F., et al., *Image-based methods for phenotyping growth dynamics and fitness components in Arabidopsis thaliana.* Plant Methods, 2018. **14**(1): p. 63.
4. Cheng, M.M., et al., *DenseCut: Densely Connected CRFs for Realtime GrabCut.* Computer Graphics Forum, 2015. **34**(7): p. 193-201.
5. Holub, E.B.B., J.L., *Symbiology of Mouse-Ear Cress (Arabidopsis thaliana) and Oomycetes.* Advances in Botanical Research, 1997. **24**: p. 227-273.
6. Schwab, R., et al., *Highly specific gene silencing by artificial microRNAs in Arabidopsis.* Plant Cell, 2006. **18**(5): p. 1121-33.
7. Hellens, R.P., et al., *pGreen: a versatile and flexible binary Ti vector for Agrobacterium-mediated plant transformation.* Plant Mol Biol, 2000. **42**(6): p. 819-32.
8. Weigel, D. and J. Glazebrook, *Arabidopsis : a laboratory manual*. 2002: Cold Spring Harbor (N.Y.) : Cold Spring Harbor laboratory press.
9. Lampropoulos, A., et al., *GreenGate - A Novel, Versatile, and Efficient Cloning System for Plant Transgenesis.* PLOS ONE, 2013. **8**(12): p. e83043.
10. Emami, S., M.-c. Yee, and J.R. Dinneny, *A robust family of Golden Gate Agrobacterium vectors for plant synthetic biology.* Frontiers in Plant Science, 2013. **4**: p. 339.
11. Wu, R., et al., *An efficient CRISPR vector toolbox for engineering large deletions in Arabidopsis thaliana.* Plant Methods, 2018. **14**(1): p. 65.